Chapter 10
The Conforming Virtual Element Method for Polyharmonic and Elastodynamics Problems: A Review

Paola F. Antonietti, Gianmarco Manzini, Ilario Mazzieri, Simone Scacchi, and Marco Verani

Abstract In this chapter we review recent results on the conforming virtual element approximation of polyharmonic and eleastodynamics problems. The structure and the content of this review is motivated by three paradigmatic examples of applications: classical and anisotropic Cahn-Hilliard equation and phase field models for brittle fracture, that are briefly discussed in the first part of the chapter. We present and discuss the mathematical details of the conforming virtual element approximation of linear polyharmonic problems, the classical Cahn-Hilliard equation and linear elastodynamics problems.

10.1 Introduction

In the recent years, there has been a tremendous interest to numerical methods that approximate partial differential equations (PDEs) on computational meshes with arbitrarily-shaped polytopal elements. One of the most successful method is the virtual element method (VEM), originally proposed in [16] for second-order elliptic problems and then extended to a wide range of applications.

The VEM was originally developed as a variational reformulation of the *nodal* mimetic finite difference (MFD) method [15, 37, 38, 73, 78] for solving partial differential equation problems on unstructured polygonal meshes. A survey on the MFD method can be found in the review paper [74] and the research mono-

P. F. Antonietti · I. Mazzieri · M. Verani (✉)
MOX, Dipartimento di Matematica, Politecnico di Milano, Milan, Italy
e-mail: paola.antonietti@polimi.it; ilario.mazzieri@polimi.it; marco.verani@polimi.it

G. Manzini
IMATI-CNR, Pavia, Italy
e-mail: marco.manzini@imati.cnr.it

S. Scacchi
Dipartimento di Matematica, Università di Milano, Milan, Italy
e-mail: simone.scacchi@unimi.it

P. F. Antonietti et al. (eds.), *The Virtual Element Method and its Applications*,
SEMA SIMAI Springer Series 31, https://doi.org/10.1007/978-3-030-95319-5_10

graph [18]. The VEM inherits the flexibility of the MFD method with respect to the admissible meshes and this feature is well reflected in the many significant applications using polytopal meshes that have been developed so far, see, for example, [6, 19, 21, 23, 24, 27, 28, 30, 45, 48, 49, 54, 82, 84, 87, 88, 94, 99]. Meanwhile, the mixed VEM for elliptic problems were introduced in setting *a la'* Raviart-Thomas in [22] and in a BDM-like setting in [39]. The nonconforming formulation for diffusion problems was proposed in [13] as the finite element reformulation of [72] and later extended to general elliptic problems [32, 47], Stokes problem [44], eigenvalue problems [63], and the biharmonic equation [7, 100]. equation [7]. Moreover, the connection between the VEM and the finite elements on polygonal/polyhedral meshes is thoroughly investigated in [43, 77], between VEM and discontinuous skeletal gradient discretizations in [55], and between the VEM and the BEM-based FEM method in [46].

The virtual element method combines a great flexibility in using polytopal meshes with a great versatility and easiness in designing approximation spaces with high-order continuity properties on general polytopal meshes. These two features turn out to be essential in the numerical treatment of the classical plate bending problem, for which a C^1-regular conforming virtual element approximation has been introduced in [36, 53]. Virtual elements with C^1- regularity have been proposed to solve elliptic problems on polygonal meshes [19] and polyedral meshes in [26], the transmission eigenvalue problem in [80], the vibration problem of Kirchhoff plates in [83], the buckling problem of Kirchhoff-Love plates in [81]. The use of C^1-virtual elements has also been employed in the conforming approximation of the Cahn-Hilliard problem [6] and the von Kármán equations [76], and in the context of residual based a posteriori error estimators for second-order elliptic problems [21].

Higher-order of regularity of the numerical approximation is also required when addressing PDEs with differential operators of order higher than two as the already mentioned biharmonic problem and the more general case of the polyharmonic equations. An example of the latter is found in the work of Reference [9].

In this chapter we consider three paradigmatic examples of applications where the conforming discretization requires highly regular approximation spaces. The first two examples are the classical and the anisotropic Cahn-Hilliard equations, that are used in modelling a wide range of problems such as the tumor growth, the origin of the Saturn rings, the separation of di-block copolymers, population dynamics, crystal growth, image processing and even the clustering of mussels, see [6] and the references therein. The third example highlights the importance of coupling phase field equations with the elastodynamic equation in the context of modelling fracture propagation (see also [3] for a phase-field besed VEM and the references therein). These three examples motivate the structure of this review, where we consider the conforming virtual approximation of the polyharmonic equation, the classical Cahn-Hilliard equation and the time-dependent elastodynamics equation.

Historically, the numerical approximation of polyharmonic problems dates back to the eighties [34], and more recently, this problem has been addressed in the context of the finite element method by [14, 62, 67, 93, 97]. The conforming virtual element approximation of the biharmonic problem has been addressed in

[36, 53]. while a non-conforming approximation has been proposed in [7, 100, 101]. In Sect. 10.2, we review the conforming virtual element approximation of polyharmonic problems following [9, 12]. A nonconforming approximation is studied in [52].

The Cahn-Hilliard equation involves fourth-order spatial derivatives and the conforming finite element method is not really popular approach because primal variational formulations of fourth-order operators requires the use of finite element basis functions that are piecewise-smooth and globally C^1-continuous. Only a few finite element formulations exists with the C^1-continuity property, see for example [57, 58], but in general, these methods are not simple and easy to implement. This high-regularity issue has successfully been addressed in the framework of isogeometric analysis [65]. The virtual element method provides a very effective framework for the design and development of highly regular conforming approximation, and in Sect. 10.3 we review the method proposed in [6].

Alternative approaches are offered by nonconforming methods [59] or discontinuous methods [98]), but these methods do not provide C^1-regular approximations. Another common strategy employed *in practice* to solve the Cahn-Hilliard equation by finite elements resorts to mixed methods; see, e.g., [56, 60, 68] for the continuous and discontinuous setting, respectively. Recently, mixed based discretization schemes on polytopal meshes have been addressed in [50] in the context of the Hybrid High Order Method, and in [75] in the context of the mixed Virtual Element Method. However, mixed finite element methods requires a bigger number of degrees of freedom, which implies, as a drawback, an increased computational cost.

Very popular strategies for numerically solving the time-dependent elastodynamics equations in the *displacement formulation* are based on spectral elements [61, 69], discontinuous Galerkin and discontinuos Galerkin spectral elements [4, 5, 91]. High-order DG methods for elastic and elasto-acoustic wave propagation problems have been extended to arbitrarily-shaped polygonal/polyhedral grids [8, 10] to further enhance the geometrical flexibility of the discontinuous Galerkin approach while guaranteeing low dissipation and dispersion errors. Recently, the lowest-order Virtual Element Method has been applied for the solution of the elastodynamics equation on nonconvex polygonal meshes [85, 86]. See also [17] for the approximation of the linear elastic problem, [20] for elastic and inelastic problems on polytope meshes, [96] for virtual element approximation of hyperbolic problems. In Sect. 10.4, we review the conforming virtual element method of arbitrary order of accuracy proposed in [11].

10.1.1 Paradigmatic Examples

In this section, we briefly describe some relevant applications whose mathematical modelling involves partial differential equations with higher order spatial operators or the combination of the elastodynamics equation and higher-order spatial partial differential equations.

10.1.1.1 Cahn-Hilliard Equation

Phase field models, which date back to the works of Korteweg [70], Cahn and Hilliard [40–42], Landau and Ginzburg [71] and van der Waals [92], have been classicaly employed to describe phase separation in binary alloys.

Consider a bounded domain $\Omega \subset \mathbb{R}^d$, $d = 1, 2, 3$, filled with components A and B presenting different properties and let $c_A(x)$ and $c_B(x)$ be their relative nonuniform mass fraction for every $x \in \Omega$. We assume that $c_i(\cdot) : \Omega \to [0, 1]$ for $i \in \{A, B\}$ and $c_A(x) + c_B(x) = 1$. Choosing one of the two functions and renaming it as $c(x)$, Cahn and Hilliard, under the additional hypothesis that the mixture is isothermal and the molar volume is uniform and independent of the pressure, proposed a model minimizing the energy functional

$$E(c) = \int_\Omega \left(F(c) + \frac{\varepsilon^2}{2} |\nabla c|^2 \right) d\mathbf{x}, \tag{10.1}$$

where $F(c)$ is the Helmholtz single-component free-energy density

$$F(c) = 2\kappa_B T_c c(1 - c) + \kappa_B T \big(c \ln(c) + (1 - c) \ln(1 - c) \big).$$

Here, κ_B is the Boltzmann constant, T the temperature and T_c the critical temperature threshold. If $T \geq T_c$ the behaviour is trivial since $F(c)$ presents a single global minimum at $c = 1/2$, and therefore the minimization of (10.1) returns a homogeneous distribution $c(x) = 1/2$ for all $x \in \Omega$. On the other hand, if $T \leq T_c$, a physically relevant double-well appears in the graph of the function.

Let us briefly comment on the structure of the energy functional (10.1). The first term takes into account the interfacial nature of the phenomenon: it increases the energy in those region of the space where both A and B are present (thus c exhibits a high gradient). The second term penalizes the measure of the interface separating the two phases. However, even if the interface separating the substances looks sharp from a macroscopic point of view, there is experimental evidence of an intermediate, diffusive, stripe; the term ε^2 is such that ε is proportional to the thickness of the stripe.

In the mathematical treatment of this problem, it is convenient to introduce the so-called *order parameter*, which we still denote by $c(x)$ and we define as $c(x) = c_A(x) - c_B(x)$ so that $c(\cdot) : \Omega \to [-1, 1]$.

Employing the order parameter, the energy functional (10.1) remains unmodified (up to a multiplicative constant), while $F(c)$ becomes

$$F(c) = -c_0 c^2 + c_1 \big((1 + c) \ln(1 + c) + (1 - c) \ln(1 - c) \big) \quad c_0 > c_1 > 0$$

as we fixed $T < T_c$. Recalling the assumption that the phenomenon mimimizes the energy (10.1) over time and denoting by $\dot{c}$ the time derivative of c, we get the

following differential description of the phenomenon

$$\dot{c} + \nabla \cdot J = 0 \quad \text{in } \Omega, \tag{10.2}$$

where the flux J is defined as

$$J = -M(c)\nabla\left(\frac{\delta E(c)}{\delta c}\right) = M(c)\nabla(F'(c) - \varepsilon^2 \Delta c).$$

The function $M(c)$ is the mobility of the substances and measures how much the molecules are free to move. The typical choices for the boundary conditions on the domain boundary Γ are:

$$n \cdot M(c)\nabla(F'(c) - \varepsilon^2 \Delta c) = 0 \quad \text{on } \Gamma, \tag{10.3}$$

$$\partial_n c = 0 \quad \text{on } \Gamma, \tag{10.4}$$

where n is the unit normal vector to Γ pointing out of Ω. The conservation of c follows from the integration of (10.2) and an application of the divergence theorem, which formally gives the relation $\partial_t \int_\Omega c \, d\mathbf{x} = 0$. In practice, the following choices for $M(c)$ and $F(c)$ are common

$$F(c) = \frac{1}{4}(c^2 - 1)^2,$$

$$M(c) = \textit{constant}.$$

Setting for simplicity $M(c) = 1$, problem (10.2) takes the simpler form of the nonlinear fourth-order parabolic equation:

$$\dot{c} + \nabla \cdot \nabla(F'(c)) - \varepsilon^2 \Delta^2 c = 0 \quad \text{in } \Omega.$$

Note the presence of the fourth-order term $\Delta^2 c$, whose numerical treatment, as it will be clear in the sequel of the paper, requires special care.

10.1.1.2 Anisotropic Cahn-Hilliard Equation

We consider the following modified free energy density

$$E(c) = \int_\Omega \frac{\gamma(n)}{\varepsilon}\left(F(c) + \frac{\varepsilon^2}{2}|\nabla c|^2\right) d\mathbf{x}, \tag{10.5}$$

where function $\gamma(n)$ describes the anisotropic property and $n = \frac{\nabla c}{|\nabla c|}$ is the interface unit normal vector. When $\gamma(n) = 1$ the H^{-1}-gradient flow of (10.5) leads to the Cahn-Hilliard equation of the previous section. In the anisotropic case, function γ

depends on n in a non-trivial way. For instance, the so-called four-fold symmetric anisotropic function is defined as follows:

$$\gamma(n) = 1 + \alpha \cos(\vartheta) \tag{10.6}$$

where ϑ is the orientation angle of the normal vector to the interface and α is the intensity of the anisotropy. For sufficiently large values of α, the corresponding Cahn-Hilliard equation becomes ill-posed and needs to be regularized [95]. To this end, we consider an extra regularizing term $\mathscr{G}(c)$ in the energy functional (10.5), which takes the form

$$E(c) = \int_\Omega \frac{\gamma(n)}{\varepsilon} \left(F(c) + \frac{\varepsilon^2}{2} |\nabla c|^2 \right) + \frac{\beta}{2} \mathscr{G}(c) \tag{10.7}$$

where $\beta > 0$ is a regularization parameter. A possible choice for the extra term $\mathscr{G}$ is the following (see, e.g., [51] for other possible choices)

$$\mathscr{G}(c) = \varepsilon |\Delta c|^2 \tag{10.8}$$

for which the corresponding H^{-1}-gradient flow of the energy (10.7) gives rise to the following *anisotropic Cahn-Hilliard* equation

$$\dot{c} - \frac{1}{\varepsilon} \Delta \left(\frac{\gamma(n)}{\varepsilon} F'(c) - \varepsilon \nabla \cdot m + \beta \varepsilon \Delta^2 c \right) = 0 \tag{10.9}$$

with

$$m = \gamma(n) \nabla c + \mathbb{P} \nabla_n \gamma(n) \left(\frac{F(c)}{\varepsilon^2 |\nabla c|} + \frac{1}{2} |\nabla c| \right)$$

where $\mathbb{P} = \mathsf{I} - n \otimes n$, I being the identity matrix and $\nabla_n \gamma(n)$ is the gradient vector containing the partial derivatives of $\gamma(n)$ with respect to the components of the normal n.

In view of the subsequent discussion on the numerical approximation of higher-order spatial differential operators, it is important to highlight the presence of the sixth-order term $\Delta^3 c$ in (10.9).

10.1.1.3 A High Order Phase Field Model for Brittle Fracture

A popular approach for the numerical solutions of fracture models is based on introducing discontinuities into the displacement field by means of remeshing or by enriching the set of basis functions by inserting discontinuities using the partition of unity method. An alternative approach is the variational approach to brittle where the solution to the fracture problem is searched as the minimizer of an

energy functional. The corresponding numerical solution hinges upon the phase-field implementation and the fracture problem is reformulated as a system of partial differential equations completely determininig the evolution of the cracks. For a short overview of these two classes of methods see, e.g., [33] and the references therein.

Recently, in [33] the variational approach to brittle fracture has been extended by proposing a fourth-order model for the phase-field approximation. The presence of higher-order derivative terms in the phase-field equation leads to a greater regularity of the solution. In the sequel, we briefly summarize the resulting differential problem so to highlight the interplay between the elastodynamics equation (cf. Eq. (10.10a) below) and the fourth-order phase field equation (cf. Eq. (10.10b) below). The unknowns of the problem are the displacement field $\mathbf{u} : \Omega \to \mathbb{R}^d$ $d = 2, 3$ and the continuous phase field variable $c : \Omega \to [0, 1]$ describing the crack ($c = 1$ away from the crack and $c = 0$ at the crack). Let λ and μ denote the usual the Lamé constants and $\epsilon = \frac{1}{2}(\nabla \mathbf{u} + \nabla \mathbf{u}^T)$ the symmetric gradient. Since ϵ is a real symmetric matrix, there exists a real orthogonal matrix P and a real diagonal matrix $\boldsymbol{\Lambda}$ such that $\boldsymbol{\epsilon} = \mathsf{P}\boldsymbol{\Lambda}\mathsf{P}^T$. We define the matrix $\boldsymbol{\Lambda}^+ = \mathrm{diag}(\langle\lambda_1\rangle, \langle\lambda_2\rangle, \langle\lambda_3\rangle)$ where $\langle x\rangle$ is the Heaviside function, the matrix $\boldsymbol{\Lambda}^- = \boldsymbol{\Lambda} - \boldsymbol{\Lambda}^+$, and the matrices $\boldsymbol{\epsilon}^\pm = \mathsf{P}\boldsymbol{\Lambda}^\pm\mathsf{P}^T$. Using these matrices, we introduce the functions

$$\psi_e^+(\boldsymbol{\epsilon}) = \frac{1}{2}\lambda\langle \mathrm{tr}\boldsymbol{\epsilon}\rangle^2 + \mu \mathrm{tr}[(\boldsymbol{\epsilon}^+)^2],$$
$$\psi_e^-(\boldsymbol{\epsilon}) = \frac{1}{2}\lambda(\mathrm{tr}\boldsymbol{\epsilon} - \langle \mathrm{tr}\boldsymbol{\epsilon}\rangle)^2 + \mu \mathrm{tr}\big((\boldsymbol{\epsilon} - \boldsymbol{\epsilon}^+)^2\big),$$

and define the stress tensor as

$$\boldsymbol{\sigma}(\mathbf{u}) = c^2 \frac{\partial \psi_e^+}{\partial \boldsymbol{\epsilon}} + \frac{\partial \psi_e^-}{\partial \boldsymbol{\epsilon}}.$$

Finally, the differential problem reads as:

$$\rho\ddot{\mathbf{u}} - \nabla \cdot \boldsymbol{\sigma}(\mathbf{u}) = \mathbf{f} \qquad \text{in } \Omega \times (0, T], \tag{10.10a}$$
$$\frac{4\ell_0 c}{g_c}\psi_e^+(\boldsymbol{\epsilon})c - 2\ell_0^2\Delta c + \ell_0^4\Delta^2 c = 1 \qquad \text{in } \Omega \times (0, T], \tag{10.10b}$$
$$\mathbf{u} = \mathbf{g}_D \qquad \text{on } \Gamma_D \times (0, T], \tag{10.10c}$$
$$\boldsymbol{\sigma}(\mathbf{u})\mathbf{n} = \mathbf{g}_N \qquad \text{on } \Gamma_N \times (0, T], \tag{10.10d}$$
$$\Delta c = 0 \qquad \text{in } \partial\Omega \times \times (0, T], \tag{10.10e}$$
$$\nabla(\ell_0^4\Delta c - 2\ell_0^2 c)\mathbf{n} = 0 \qquad \text{in } \partial\Omega \times \times (0, T], \tag{10.10f}$$
$$(\mathbf{u}, \dot{\mathbf{u}}) = (\mathbf{u}_0, \mathbf{u}_1) \qquad \text{in } \Omega \times \{0\}, \tag{10.10g}$$

where we split $\partial\Omega = \Gamma_D \cup \Gamma_N$ for the Dirichlet and Neumann boundary conditions, and $\ell_0 > 0$ is suitable length scale parameter.

10.1.2 Notation and Technicalities

Throughout the paper, we consider the usual multi-index notation. In particular, if v is a sufficiently regular bivariate function and $\alpha = (\alpha_1, \alpha_2)$ a multi-index with α_1, α_2 nonnegative integer numbers, the function $D^\alpha v = \partial^{|\alpha|} v / \partial x_1^{\alpha_1} \partial x_2^{\alpha_2}$ is the partial derivative of v of order $|\alpha| = \alpha_1 + \alpha_2 > 0$. For $\alpha = (0, 0)$, we adopt the convention that $D^\alpha v$ coincides with v. Also, for the sake of exposition, we may use the shortcut notation $\partial_x v$, $\partial_y v$, $\partial_{xx} v$, $\partial_{xy} v$, $\partial_{yy} v$, to denote the first- and second-order partial derivatives along the coordinate directions x and y; $\partial_n v$, $\partial_t v$, $\partial_{nn} v$, $\partial_{nt} v$, $\partial_{tt} v$ to denote the first- and second-order normal and tangential derivatives along a given mesh edge; and $\partial_n^m v$ and $\partial_t^m v$ to denote the normal and tangential derivative of v of order m along a given mesh edge. Finally, let $\mathbf{n} = (n_x, n_y)$ and $\boldsymbol{\tau} = (\tau_x, \tau_y)$ be the unit normal and tangential vectors to a given edge e of an arbitrary polygon P, respectively. We recall the following relations between the first derivatives of v:

$$\partial_n v = \nabla v^T \mathbf{n} = n_x \partial_x v + n_y \partial_y v, \quad \partial_\tau v = \nabla v^T \boldsymbol{\tau} = \tau_x \partial_x v + \tau_y \partial_y v, \tag{10.11}$$

and the second derivatives of v:

$$\partial_{nn} v = \mathbf{n}^T \mathsf{H}(v) \mathbf{n}, \quad \partial_{n\tau} v = \mathbf{n}^T \mathsf{H}(v) \boldsymbol{\tau}, \quad \partial_{\tau\tau} v = \boldsymbol{\tau}^T \mathsf{H}(v) \boldsymbol{\tau}, \tag{10.12}$$

respectively, where the matrix $\mathsf{H}(v)$ is the Hessian of v, i.e., $\mathsf{H}_{11}(v) = \partial_{xx} v$, $\mathsf{H}_{12}(v) = \mathsf{H}_{21}(v) = \partial_{xy} v$, $\mathsf{H}_{22}(v) = \partial_{yy} v$.

We use the standard definitions and notation of Sobolev spaces, norms and seminorms [1]. Let k be a nonnegative integer number. The Sobolev space $H^k(\omega)$ consists of all square integrable functions with all square integrable weak derivatives up to order k that are defined on the open bounded connected subset ω of $\mathbb{R}^2$. As usual, if $k = 0$, we prefer the notation $L^2(\omega)$. Norm and seminorm in $H^k(\omega)$ are denoted by $\|\cdot\|_{k,\omega}$ and $|\cdot|_{k,\omega}$, respectively, and $(\cdot,\cdot)_\omega$ denote the L^2-inner product. We omit the subscript ω when ω is the whole computational domain Ω.

Given the mesh partitioning $\Omega_h = \{\mathsf{P}\}$ of the domain Ω into elements P, we define the broken (scalar) Sobolev space for any integer $k > 0$

$$H^k(\Omega_h) = \prod_{\mathsf{P}\in\Omega_h} H^k(\mathsf{P}) = \left\{ v \in L^2(\Omega) \,:\, v_{|\mathsf{P}} \in H^k(\mathsf{P}) \right\},$$

which we endow with the broken H^k-norm

$$\|v\|_{k,h}^2 = \sum_{\mathsf{P}\in\Omega_h} \|v\|_{k,\mathsf{P}}^2 \qquad \forall\, v \in H^k(\Omega_h), \tag{10.13}$$

and, for $k = 1$, with the broken H^1-seminorm

$$|v|_{1,h}^2 = \sum_{\mathsf{P}\in\Omega_h} \|\nabla v\|_{0,\mathsf{P}}^2 \qquad \forall\, v \in H^1(\Omega_h). \tag{10.14}$$

We denote the linear space of polynomials of degree up to ℓ defined on ω by $\mathbb{P}_\ell(\omega)$, with the useful conventional notation that $\mathbb{P}_{-1}(\omega) = \{0\}$. We denote the space of two-dimensional vector polynomials of degree up to ℓ on ω by $\left[\mathbb{P}_\ell(\omega)\right]^2$; the space of symmetric 2×2-sized tensor polynomials of degree up to ℓ on ω by $\mathbb{P}^{2\times 2}_{\ell,\mathrm{sym}}(\omega)$. Space $\mathbb{P}_\ell(\omega)$ is the span of the finite set of *scaled monomials of degree up to* ℓ, that are given by

$$\mathscr{M}_\ell(\omega) = \left\{ \left(\frac{\mathbf{x}-\mathbf{x}_\omega}{h_\omega}\right)^\alpha \text{ with } |\alpha| \le \ell \right\},$$

where

- $\mathbf{x}_\omega$ denotes the center of gravity of ω and h_ω its characteristic length, as, for instance, the edge length or the cell diameter for $d = 1, 2$;
- $\alpha = (\alpha_1, \alpha_2)$ is the two-dimensional multi-index of nonnegative integers α_i with degree $|\alpha| = \alpha_1 + \alpha_2 \le \ell$ and such that $\mathbf{x}^\alpha = x_1^{\alpha_1} x_2^{\alpha_2}$ for any $\mathbf{x} \in \mathbb{R}^2$.

We will also use the set of *scaled monomials of degree exactly equal to* ℓ, denoted by $\mathscr{M}_\ell^*(\omega)$ and obtained by setting $|\alpha| = \ell$ in the definition above.

Finally, we use the letter C in the estimates below to denote a strictly positive constant whose value can change at any instance but that is independent of the discretization parameters such as the mesh size h. Note that C may depend on the the polynomial order, on the constants of the model equations or the variational problem, like the coercivity and continuity constants, or even constants that are uniformly defined for the family of meshes of the approximation while $h \to 0$, such as the mesh regularity constant, the stability constants of the discrete bilinear forms, etc. Whenever it is convenient, we will simplify the notation by using expressions like $x \lesssim y$ and $x \gtrsim y$ to mean that $x \le Cy$ and $x \ge Cy$, respectively, C being the generic constant in the sense defined above.

10.1.3 Mesh Assumptions

Throughout the paper we assume that $\mathscr{T} = \{\Omega_h\}_h$ is a family of decompositions of the computational domain Ω, where each mesh Ω_h is a collection of nonoverlapping polygonal elements P with boundary $\partial\mathsf{P}$, such that $\bar{\Omega} = \mathbb{U}_{\mathsf{P}\in\Omega_h} \bar{\mathsf{P}}$. Each mesh is labeled by the *mesh size* h, the diameter of the mesh, defined as usual by $h = \max_{\mathsf{P}\in\Omega_h} h_\mathsf{P}$, where $h_\mathsf{P} = \sup_{\mathbf{x},\mathbf{y}\in\mathsf{P}} |\mathbf{x}-\mathbf{y}|$. We assume the mesh sizes of family $\mathscr{T}$ form a countable subset of $\mathscr{H} = (0, \infty)$ having zero as its unique accumulation

point. We denote the set of mesh vertices v by $\mathscr{V}_h$ and the set of mesh edges e by $\mathscr{E}_h$ Moreover, the symbol h_{V} is a characteristic lenght associated with each vertex; more precisely, h_{V} is the average of the diameters of the polygons sharing vertex v. We consider the following mesh regularity assumptions:

(M) There exists a positive constant γ, *mesh regularity constant*, which is independent of h (and P) and such that for $K \in \Omega_h$ there hold:

- **(M1)** P is star-shaped with respect to every point of a ball of radius γh_{P}, where h_{P} is the diameter of P;
- **(M2)** for every edge e of the cell boundary $\partial\mathsf{P}$ of every cell P of Ω_h, it holds that $h_{\mathrm{e}} \geq \gamma h_{\mathsf{P}}$, where h_{e} denotes the length of e.

All the results contained in the rest of the paper are obtained under assumptions **(M1)**–**(M2)**.

10.2 The Virtual Element Method for the Polyharmonic Problem

10.2.1 The Continuous Problem

Let $\Omega \subset \mathbb{R}^2$ be a open, bounded, convex domain with polygonal boundary Γ. For any integer $p \geq 1$, we introduce the conforming virtual element method for the approximation of the following problem:

$$(-\Delta)^p u = f \qquad \text{in } \Omega, \tag{10.1a}$$

$$\partial_n^j u = 0 \qquad \text{for } j = 0, \ldots, p-1 \text{ on } \Gamma, \tag{10.1b}$$

(recall the conventional notation $\partial_n^0 u = u$). Let

$$V \equiv H_0^p(\Omega) = \left\{ v \in H^p(\Omega) : \partial_n^j v = 0 \text{ on } \Gamma,\ j = 0, \ldots, p-1 \right\}.$$

Denoting the duality pairing between V and its dual V' by $\langle \cdot, \cdot \rangle$, the variational formulation of the polyharmonic problem (10.1) reads as: *Find $u \in V$ such that*

$$a(u, v) = \langle f, v \rangle \qquad \forall v \in V, \tag{10.2}$$

where, for any nonnegative integer ℓ, the bilinear form is given by:

$$a(u, v) = \begin{cases} \int_\Omega \nabla\Delta^\ell u \cdot \nabla\Delta^\ell v \, d\mathbf{x} & \text{for } p = 2\ell + 1, \\ \int_\Omega \Delta^\ell u \, \Delta^\ell v \, d\mathbf{x} & \text{for } p = 2\ell. \end{cases} \tag{10.3}$$

Whenever $f \in L^2(\Omega)$ we have

$$\langle f, v \rangle = (f, v) = \int_\Omega f v \, dV \, d\mathbf{x}. \tag{10.4}$$

where $(\cdot, \cdot)$ denotes the L^2-inner product. The existence and uniqueness of the solution to (10.2) follows from the Lax-Milgram Theorem because of the continuity and coercivity of the bilinear form $a(\cdot, \cdot)$ with respect to $\|\cdot\|_V = |\cdot|_{p,\Omega}$ which is a norm on $H_0^p(\Omega)$. Moreover, since Ω is a convex polygon, from [64] we know that $u \in H^{2p-m}(\Omega) \cap H_0^p(\Omega)$ if $f \in H^{-m}(\Omega)$, $m \leq p$ and it holds that $\|u\|_{2p-m} \leq C\|f\|_{-m}$. In the following, we denote the coercivity and continuity constants of $a(\cdot, \cdot)$ by α and M, respectively.

Let P be a polygonal element and set

$$a_{\mathsf{P}}(u, v) = \begin{cases} \int_{\mathsf{P}} \nabla \Delta^\ell u \cdot \nabla \Delta^\ell v \, d\mathbf{x} & \text{for } p = 2\ell + 1, \\ \int_{\mathsf{P}} \Delta^\ell u \, \Delta^\ell v \, d\mathbf{x} & \text{for } p = 2\ell. \end{cases}$$

For an odd p, i.e., $p = 2\ell + 1$, a repeated application of the integration by parts formula yields

$$\begin{aligned} a_{\mathsf{P}}(u, v) = &- \int_{\mathsf{P}} \Delta^p u \, v \, d\mathbf{x} + \int_{\partial \mathsf{P}} \partial_n(\Delta^\ell u) \, \Delta^\ell v \, ds \\ &+ \sum_{i=1}^{\ell} \left(\int_{\partial \mathsf{P}} \partial_n(\Delta^{p-i} u) \, \Delta^{i-1} v \, ds - \int_{\partial \mathsf{P}} \Delta^{p-i} u \, \partial_n(\Delta^{i-1} v) \, ds \right), \end{aligned} \tag{10.5}$$

while, for an even p, i.e., $p = 2\ell$, we have

$$\begin{aligned} a_{\mathsf{P}}(u, v) = &\int_{\mathsf{P}} \Delta^p u \, v \, d\mathbf{x} \\ &+ \sum_{i=1}^{\ell} \left(\int_{\partial \mathsf{P}} \partial_n(\Delta^{p-i} u) \, \Delta^{i-1} v \, ds - \int_{\partial \mathsf{P}} \Delta^{p-i} u \, \partial_n(\Delta^{i-1} v) \, ds \right). \end{aligned} \tag{10.6}$$

10.2.2 The Conforming Virtual Element Approximation

The conforming virtual element discretization of problem (10.2) hinges upon three mathematical objects: (1) the finite dimensional conforming virtual element space

$V_{h,r}^p \subset V$; (2) the continuous and coercive discrete bilinear form $a_h(\cdot,\cdot)$; (3) the linear functional $\langle f_h, \cdot \rangle$.

Using such objects, we formulate the virtual element method as: *Find* $u_h \in V_{h,r}^p$ *such that*

$$a_h(u_h, v_h) = \langle f_h, v_h \rangle \quad \forall v_h \in V_{h,r}^p. \tag{10.7}$$

The existence and uniqueness of the solution u_h is again a consequence of the Lax-Milgram theorem [35, Theorem 2.7.7, page 62].

10.2.2.1 Virtual Element Spaces

For $p \geq 1$ and $r \geq 2p-1$, the local Virtual Element space on element P is defined by

$$V_{h,r}^p(\mathsf{P}) = \Big\{ v_h \in H^p(\mathsf{P}) : \Delta^p v_h \in \mathbb{P}_{r-2p}(\mathsf{P}),\ v_h \in \mathbb{P}_r(\mathsf{e}),\ \partial_n^i v_h \in \mathbb{P}_{r-i}(\mathsf{e}),\ i = 1, \dots, p-1\ \forall \mathsf{e} \in \partial\mathsf{P} \Big\},$$

with the conventional notation that $\mathbb{P}_{-1}(\mathsf{P}) = \{0\}$. The virtual element space $V_{h,r}^p(\mathsf{P})$ contains the space of polynomials $\mathbb{P}_r(\mathsf{P})$, for $r \geq 2p-1$. Moreover, for $p = 1$, it coincides with the conforming virtual element space for the Poisson equation [16], and for $p = 2$, it coincides with the conforming virtual element space for the biharmonic equation [36]. The requirement $v_h \in H^p(\mathsf{P})$ implies that suitable compatibility conditions for v_h and its derivatives up to order $p-1$ must hold at the vertices of the polygon (see, e.g., [66, Theorems 1.5.2.4 and 1.5.7.8] and [29, Section 5]).

We characterize the functions in $V_{h,r}^p(\mathsf{P})$ through the following set of *degrees of freedom*:

- **(D1)** $h_{\mathsf{v}}^{|\nu|} D^\nu v_h(\mathsf{v})$, $|\nu| \leq p-1$ for any vertex v of the polygonal boundary $\partial\mathsf{P}$;
- **(D2)** $h_{\mathsf{e}}^{-1} \displaystyle\int_{\mathsf{e}} q\, v_h\, ds$ for any $q \in \mathbb{P}_{r-2p}(\mathsf{e})$ and any edge e of the polygonal boundary $\partial\mathsf{P}$;
- **(D3)** $h_{\mathsf{e}}^{-1+j} \displaystyle\int_{\mathsf{e}} q\, \partial_n^j v_h\, ds$ for any $q \in \mathbb{P}_{r-2p+j}(\mathsf{e})$, $j = 1, \dots, p-1$ and any edge e of $\partial\mathsf{P}$;
- **(D4)** $h_{\mathsf{P}}^{-2} \displaystyle\int_{\mathsf{P}} q_h v_h\ d\mathbf{x}$ for any $q \in \mathbb{P}_{r-2p}(\mathsf{P})$.

Here, as usual, we assume that $\mathbb{P}_{-n}(\cdot) = \{0\}$ for $n \geq 1$. Figure 10.1 illustrates the degrees of freedom on a given edge e for $p = 1, 2, 3$ (Laplace, biharmonic, and triharmonic case) and $r = 2p-1, 2p$; the corresponding internal degrees of freedom (D4) are absent in the case $r = 2p-1$, while reduce to a single one in the

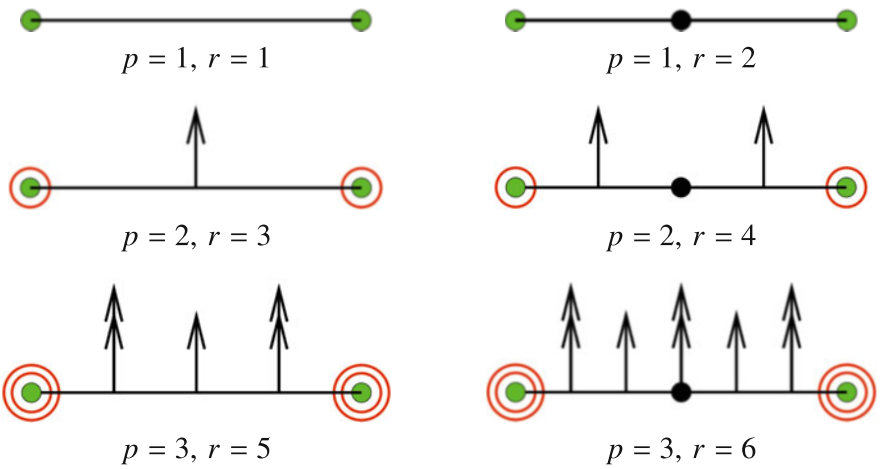

Fig. 10.1 Edge degrees of freedom of the Virtual Element space $V_{h,r}^p(\mathsf{P})$ for the polyharmonic problem with $p = 1$ (top panels, Laplace operator), $p = 2$ (middle panels, bi-harmonic operator), $p = 3$ (bottom panels, tri-harmonic operator). Here, p is the order of the partial differential operator; $r = 1, 2, \ldots, 6$ are the integer parameters that specify the degree of the polynomial subspace $\mathbb{P}_r(\mathsf{P})$ of the VEM space $V_{h,r}^3(\mathsf{P})$. The (green) dots at the vertices represent the vertex values and each (red) vertex circle represents an order of derivation. The (black) dot on the edge represents the moment of $v_{h|e}$; the arrows represent the moments of $\partial_n v_{h|e}$; the double arrows represent the moments of $\partial_{nn} v_{h|e}$. The corresponding internal degrees of freedom (D4) are absent in the case $r = 2p - 1$, while reduce to a single one in the case $r = 2p$

case $r = 2p$. Finally, we note that in general the internal degrees of freedom **(D4)** make it possible to define the L^2-orthogonal polynomial projection of v_h onto the space of polynomial of degree $r - 2p$.

The dimension of $V_{h,r}^p(\mathsf{P})$ is

$$d(V_{h,r}^p(\mathsf{P})) = \frac{p(p+1)}{2} N^{\mathscr{P}} + N^{\mathscr{P}} \sum_{j=0}^{p-1} (r - 2p + j + 1) + \frac{(r - 2p + 1)(r - 2p + 2)}{2},$$

where $N^{\mathscr{P}}$ is the number of vertices, which equals the number of edges, of P.

In [9], it is proved that the above choice of degrees of freedom is unisolvent in $V_{h,r}^p(\mathsf{P})$.

Building upon the local spaces $V_{h,r}^p(\mathsf{P})$ for all $\mathsf{P} \in \Omega_h$, the *global* conforming virtual element space $V_{h,r}^p$ is defined on Ω as

$$V_{h,r}^p = \left\{ v_h \in H_0^p(\Omega) \,:\, v_{h|\mathsf{P}} \in V_{h,r}^p(\mathsf{P}) \;\forall \mathsf{P} \in \Omega_h \right\}. \tag{10.8}$$

We remark that the associated global space is made of $H^p(\Omega)$ functions. Indeed, the restriction of a virtual element function v_h to each element P belongs to $H^p(\mathsf{P})$ and

glues with C^{p-1}-regularity across the internal mesh faces. The set of global degrees of freedom inherited by the local degrees of freedom are:

- $h_{\mathsf{V}}^{|\nu|} D^{\nu} v_h(\mathsf{v})$, $|\nu| \leq p-1$ for every interior vertex v of Ω_h;
- $h_{\mathrm{e}}^{-1} \displaystyle\int_{\mathrm{e}} q\, v_h \, ds$ for any $q \in \mathbb{P}_{r-2p}(\mathrm{e})$ and every interior edge $\mathrm{e} \in \mathscr{E}_h$;
- $h_{\mathrm{e}}^{-1+j} \displaystyle\int_{\mathrm{e}} q\, \partial_n^j v_h \, ds$ for any $q \in \mathbb{P}_{r-2p+j}(e)$ $j = 1, \ldots, p-1$ and every interior edge $\mathrm{e} \in \mathscr{E}_h$;
- $h_{\mathsf{P}}^{-2} \displaystyle\int_{\mathsf{P}} q\, v_h \, d\mathbf{x}$ for any $q \in \mathbb{P}_{r-2p}(\mathsf{P})$ and every $\mathsf{P} \in \Omega_h$.

10.2.2.2 Modified Lowest Order Virtual Element Spaces

In this section, we briefly discuss the possibility of introducing modified lowest order virtual element spaces with a reduced number of degrees of freedom with respect to the corresponding lowest order ones that were introduced previously. The price we pay is a reduced order of accuracy since the polynomial functions included in such modified spaces has a lower degree.

For the sake of presentation we start from the case $p = 3$, while we refer the reader to [36] for the case of $p = 2$ and Sect. 10.3.2.1 where the reduced virtual space is employed in the context of the approximation of the Cahn-Hilliard problem. Consider the modified local virtual element space:

$$\tilde{V}_{h,5}^3(\mathsf{P}) = \Big\{ v_h \in H^3(\mathsf{P}) \,:\, \Delta^3 v_h = 0,\, v_h \in \mathbb{P}_5(\mathrm{e}),\, \partial_n v_h \in \mathbb{P}_3(\mathrm{e}),\, \partial_{nn} v_h \in \mathbb{P}_2(\mathrm{e})\ \forall \mathrm{e} \in \partial\mathsf{P} \Big\}$$

with associated degrees of freedom:

(D1') $h_{\mathsf{V}}^{|\nu|} D^{\nu} v_h(\mathsf{v})$, $|\nu| \leq 2$ for any vertex v of $\partial\mathsf{P}$;

(D2') $h_{\mathrm{e}} \displaystyle\int_{\mathrm{e}} \partial_{nn} v_h \, ds$ for any edge e of $\partial\mathsf{P}$.

In Ref. [9], we proved that the degrees of freedom **(D1')** and **(D2')** are unisolvent in $\tilde{V}_{h,5}^3(\mathsf{P})$ and this space contains the linear subspace of polynomials of degree up to 4. Moreover, the associated global space obtained by gluing together all the elemental spaces $\tilde{V}_{h,5}^3(\mathsf{P})$ reads as:

$$\tilde{V}_{h,5}^3 = \Big\{ v_h \in H_0^3(\Omega) \,:\, v_h|_{\mathsf{P}} \in \tilde{V}_{h,5}^3(\mathsf{P})\ \forall \mathsf{P} \in \Omega_h \Big\}, \tag{10.9}$$

is made of $H^3(\Omega)$ functions.

Analogously, in the general case we can build the modified lowest order spaces containing the space of polynomials of degree up to $2p-2$:

$$\tilde{V}^p_{h,2p-1}(\mathsf{P}) = \Big\{ v_h \in H^p(\mathsf{P}) : \Delta^p v_h = 0,\, v_h \in \mathbb{P}_{2p-1}(\mathrm{e}),\, \partial_n^i v_h \in \mathbb{P}_{2p-2-i}(\mathrm{e}), \\ i = 1, \ldots, p-1 \;\forall \mathrm{e} \in \partial\mathsf{P} \Big\},$$

with associated degrees of freedom:

(D1') $h_{\mathsf{V}}^{|\nu|} D^\nu v_h(\mathsf{v})$, $|\nu| \le p-1$ for any vertex v of $\partial\mathsf{P}$;

(D2') $h_{\mathrm{e}}^{-1+j} \displaystyle\int_{\mathrm{e}} q\, \partial_n^i v_h \, ds$ for any $q \in \mathbb{P}_{j-2}(\mathrm{e})$ and edge e of $\partial\mathsf{P}$, $j = 1, \ldots, p-1$.

10.2.2.3 Discrete Bilinear Form

To define the elliptic projection $\Pi_r^{\nabla,\mathsf{P}} : V^p_{h,r}(\mathsf{P}) \to \mathbb{P}_r(\mathsf{P})$, we first need to introduce the *vertex average projector* $\widehat{\Pi}^{\mathsf{P}} : V^p_{h,r}(\mathsf{P}) \to \mathbb{P}_0(\mathsf{P})$, which projects any smooth enough function defined on P onto the space of constant polynomials. To this end, consider the continuous function ψ defined on P. The *vertex average projection* of ψ onto the constant polynomial space is given by:

$$\widehat{\Pi}^{\mathsf{P}} \psi = \frac{1}{N^{\mathscr{P}}} \sum_{\mathsf{v} \in \partial\mathsf{P}} \psi(\mathsf{v}). \tag{10.10}$$

Finally, we define the elliptic projection $\Pi_r^{\nabla,\mathsf{P}} : V^p_{h,r}(\mathsf{P}) \to \mathbb{P}_r(\mathsf{P})$ as the solution of the following finite dimensional variational problem

$$a_{\mathsf{P}}(\Pi_r^{\nabla,\mathsf{P}} v_h, q) = a_{\mathsf{P}}(v_h, q) \qquad \forall q \in \mathbb{P}_r(\mathsf{P}), \tag{10.11}$$

$$\widehat{\Pi}^{\mathsf{P}} D^\nu \Pi_r^{\nabla,\mathsf{P}} v_h = \widehat{\Pi}^{\mathsf{P}} D^\nu v_h \qquad |\nu| \le p-1. \tag{10.12}$$

According to Reference [9], such operator has two important properties:

(i) it is a polynomial-preserving operator in the sense that $\Pi_r^{\nabla,\mathsf{P}} q = q$ for every $q \in \mathbb{P}_r(\mathsf{P})$;

(ii) $\Pi_r^{\nabla,\mathsf{P}} v_h$ is *computable* using only the degrees of freedom of v_h.

We write the symmetric bilinear form $a_h : V^p_{h,r} \times V^p_{h,r} \to \mathbb{R}$ as the sum of local terms

$$a_h(u_h, v_h) = \sum_{\mathsf{P} \in \Omega_h} a_{h,\mathsf{P}}(u_h, v_h), \tag{10.13}$$

where each local term $a_{h,\mathsf{P}} : V_{h,r}^p(\mathsf{P}) \times V_{h,r}^p(\mathsf{P}) \to \mathbb{R}$ is a symmetric bilinear form. We set

$$a_{h,\mathsf{P}}(u_h, v_h) = a_{\mathsf{P}}(\Pi_r^{\nabla,\mathsf{P}} u_h, \Pi_r^{\nabla,\mathsf{P}} v_h) + S^{\mathsf{P}}(u_h - \Pi_r^{\nabla,\mathsf{P}} u_h, v_h - \Pi_r^{\nabla,\mathsf{P}} v_h), \tag{10.14}$$

where $S^{\mathsf{P}} : V_{h,r}^p(\mathsf{P}) \times V_{h,r}^p(\mathsf{P}) \to \mathbb{R}$ is a symmetric positive definite bilinear form such that

$$\sigma_* a_{\mathsf{P}}(v_h, v_h) \leq S^{\mathsf{P}}(v_h, v_h) \leq \sigma^* a_{\mathsf{P}}(v_h, v_h) \qquad \forall v_h \in V_{h,r}^p(\mathsf{P}) \text{ with } \Pi_r^{\nabla,\mathsf{P}} v_h = 0, \tag{10.15}$$

for two some positive constants σ_*, σ^* independent of h and P. The bilinear form $a_{h,\mathsf{P}}(\cdot,\cdot)$ has the two fundamental properties of *r-consistency* and *stability* [9]:

(*i*) *r*-**Consistency**: for every polynomial $q \in \mathbb{P}_r(\mathsf{P})$ and function $V_{h,r}^p(\mathsf{P})$ we have:

$$a_{h,\mathsf{P}}(v_h, q) = a_{\mathsf{P}}(v_h, q); \tag{10.16}$$

(*ii*) **Stability**: there exist two positive constants α_*, α^* independent of h and P such that for every $v_h \in V_{h,r}^p(\mathsf{P})$ it holds:

$$\alpha_* a_{\mathsf{P}}(v_h, v_h) \leq a_{h,\mathsf{P}}(v_h, v_h) \leq \alpha^* a_{\mathsf{P}}(v_h, v_h). \tag{10.17}$$

10.2.2.4 Discrete Load Term

We denote by f_h the piecewise polynomial approximation of f on Ω_h given by

$$f_{h|\mathsf{P}} = \Pi_{r-p}^{0,\mathsf{P}} f, \tag{10.18}$$

for $r \geq 2p - 1$ and $\mathsf{P} \in \Omega_h$. Then, we set

$$\langle f_h, v_h \rangle = \sum_{\mathsf{P} \in \Omega_h} \int_{\mathsf{P}} f_h v_h \, d\mathbf{x} \tag{10.19}$$

which implies, using the L^2-orthogonal projection, that

$$\langle f_h, v_h \rangle = \sum_{\mathsf{P} \in \Omega_h} \int_{\mathsf{P}} \Pi_{r-p}^{0,\mathsf{P}} f \, \Pi_{r-p}^{0,\mathsf{P}} v_h \, d\mathbf{x} = \sum_{\mathsf{P} \in \Omega_h} \int_{\mathsf{P}} f \, \Pi_{r-p}^{0,\mathsf{P}} v_h \, d\mathbf{x}. \tag{10.20}$$

The right-hand side of (10.20) is computable by a combined use of the degrees of freedom **(D1)–(D4)** and the enhanced approach of Reference [2].

10.2.2.5 VEM Spaces with Arbitrary Degree of Continuity

In this section we briefly sketch the construction of global virtual element spaces with arbitrary high order of continuity. More precisely, we consider the local virtual element space defined as before, for $r \geq 2p-1$:

$$V_{h,r}^{p}(\mathsf{P}) = \Big\{ v_h \in H^p(\mathsf{P}) : \Delta^p v_h \in \mathbb{P}_{r-2p}(\mathsf{P}),\ v_h \in \mathbb{P}_r(\mathrm{e}),\ \partial_n^j v_h \in \mathbb{P}_{r-j}(\mathrm{e}),\ j = 1, \ldots, p-1\ \forall \mathrm{e} \in \partial\mathsf{P} \Big\}.$$

Differently from the previous section, we make the degrees of freedom depend on a given parameter t with $0 \leq t \leq p-1$. For a given value of t we choose the *degrees of freedom* as follows

(D1) $h_{\mathsf{V}}^{|\nu|} D^{\nu} v_h(\mathsf{v})$, $|\nu| \leq p-1$ for any vertex v of P;

(D2) $h_{\mathrm{e}}^{-1} \displaystyle\int_{\mathrm{e}} v_h q \, ds$ for any $q \in \mathbb{P}_{r-2p}(\mathrm{e})$, for any edge e of $\partial\mathsf{P}$;

(D3) $h_{\mathrm{e}}^{-1+j} \displaystyle\int_{\mathrm{e}} \partial_n^j v_h q \, ds$ for any $q \in \mathbb{P}_{r-2p+j}(\mathrm{e})$ and edge $\mathrm{e} \in \partial\mathsf{P}$, $j = 1, \ldots, p-1$;

(D4') $h_{\mathsf{P}}^{-2} \displaystyle\int_{\mathsf{P}} q\, v_h \, d\mathbf{x}$ for any $q \in \mathbb{P}_{r-2(p-t)}(\mathsf{P})$;

where as usual we assume $\mathbb{P}_{-n}(\cdot) = \{0\}$ for $n = 1, 2, 3, \ldots$.

This set of degrees is still unisolvent, cf. [9]. Moreover, for $r \geq 2p-1$ it holds that $\mathbb{P}_r(\mathsf{P}) \subset V_{h,r}^{p}(\mathsf{P})$. Finally, it is worth noting that the choice **(D4')**, if compared with **(D4)**, still guarantees that the associated global space is made of C^{p-1} functions.

However, in this latter case we can use the degrees of freedom **(D1)–(D4')** to solve a differential problem involving the Δ^{p-t} operator and $C^{p-1}(\Omega)$ basis functions. For the sake of exposition, let us consider the following two examples, in the context of the Laplacian and the Bilaplacian problem.

1. Choosing p and t such that $p - t = 1$ we obtain a C^{p-1}-conforming virtual element method for the solution of the Laplacian problem. For example, for $p = 3, t = 2$ and $r = 5$, the local space $V_{h,5}^{3}(\mathsf{P})$ endowed with the corresponding degrees of freedom **(D1)–(D4')** can be employed to build a global space made of C^2 functions. It is also worth mentioning that the new choice **(D4')**, differently from the original choice **(D4)**, is essential for the computability of the elliptic projection, see (10.11)–(10.12), with respect to the bilinear form $a_{\mathsf{P}}(\cdot,\cdot) = \int_{\mathsf{P}} \nabla(\cdot)\nabla(\cdot)\, d\mathbf{x}$.

2. Choosing p and t such that $p - t = 2$ we have a C^{p-1}-conforming virtual element method for the solution of the Bilaplacian problem. For example, for $p = 3$, $t = 1$ and $r = 5$, similarly to the previous case, the space $V^3_{h,5}(\mathsf{P})$ together with **(D1)**–**(D4')** provides a global space of C^2 functions that can be employed for the solution of the biharmonic problem.

It is worth remembering that C^1-regular virtual element basis function has been employed, e.g., in [21] to study residual based a posteriori error estimators for the virtual element approximation of second order elliptic problems. Moreover, the solution of coupled elliptic problems of different order can take advantage from this flexibility of the degree of continuity of the basis functions. Indeed, for the sake of clarity consider the conforming virtual element approximation of the following simplified situation:

$$\begin{aligned}
-\Delta u_1 &= f_1 && \text{in } \Omega_1,\\
\Delta^2 u_2 &= f_2 && \text{in } \Omega_2,\\
u_1 &= u_2 && \text{on } \Gamma = \Omega_1 \cap \Omega_2,\\
\partial_n u_1 &= \partial_n u_2 && \text{on } \Gamma,\\
u_1 &= 0 && \text{on } \partial\Omega_1 \setminus \Gamma,\\
u_2 &= 0 && \text{on } \partial\Omega_2 \setminus \Gamma,\\
\partial_n u_2 &= 0 && \text{on } \partial\Omega_2 \setminus \Gamma.
\end{aligned}$$

Handling the coupling conditions on Γ asks for the use of C^1-regular virtual basis functions not only in Ω_2 where the bilaplacian problem is defined, but also in Ω_1, where the second order elliptic problem is defined. Indeed, a simple use of C^0-basis functions in Ω_1, which would be natural given the second order of the problem, would not allow the imposition (or at least a simple imposition) of the gluing condition on the normal derivatives.

10.2.2.6 Convergence Results

The following convergence result in the energy norm holds (see [9] for the proof).

Theorem 10.1 *Let $f \in H^{r-p+1}(\Omega)$ be the forcing term at the right-hand side, u the solution of the variational problem (10.2) and $u_h \in V^p_{h,r}$ the solution of the virtual element method (10.7). Then, it holds that*

$$\|u - u_h\|_V \leq Ch^{r-(p-1)}\big(|u|_{r+1} + |f|_{r-p+1}\big). \tag{10.21}$$

Moreover, the following convergence results in lower order norms can established [9].

Theorem 10.2 (Even p, Even Norms) *Let $f \in H^{r-p+1}(\Omega)$, u the solution of the variational problem (10.2) with $p = 2\ell$ and $v_h \in V_{h,r}^p$ the solution of the virtual element method (10.7). Then, there exists a positive constant C independent of h such that*

$$|u - u_h|_{2i} \leq Ch^{r+1-2i}\Big(|u|_{r+1} + |f|_{r-(p-1)}\Big), \tag{10.22}$$

for every integer $i = 0, \ldots, \ell - 1$.

Theorem 10.3 (Even p, Odd Norms) *Let $f \in H^{r-p+1}(\Omega)$, and u the solution of the variational problem (10.2) with $p = 2\ell$ and $u_h \in V_{h,r}^p$ the solution of the virtual element method (10.7). Then, there exists a positive constant C independent of h such that*

$$|u - u_h|_{2i+1} \leq Ch^{(r+1)-(2i+1)}\Big(|u|_{r+1} + |f|_{r-(p-1)}\Big), \tag{10.23}$$

for every integer $i = 0, \ldots, \ell - 1$.

Theorem 10.4 (Odd p, Even Norms) *Let u be the solution of the variational problem (10.2) and $u_h \in V_{h,r}^p$ the solution of the virtual element method (10.7). Then, there exists a positive constant C independent of h such that*

$$|u - u_h|_{2i} \leq Ch^{(r+1)-2i}\Big(|u|_{r+1} + |f|_{r-(p-1)}\Big), \tag{10.24}$$

for every integer $i = 0, \ldots, \ell - 1$.

Theorem 10.5 (Odd p, Odd Norms) *Let u be the solution of the variational problem (10.2) and $u_h \in V_{h,r}^p$ the solution of the virtual element method (10.7). Then, there exists a positive constant C independent of h such that*

$$|u - u_h|_{2i+1} \leq Ch^{(r+1)-(2i+1)}\Big(|u|_{r+1} + |f|_{r-(p-1)}\Big), \tag{10.25}$$

for every integer $i = 0, \ldots, \ell - 1$.

10.3 The Virtual Element Method for the Cahn-Hilliard Problem

10.3.1 The Continuous Problem

Let $\Omega \subset \mathbb{R}^2$ be an open, bounded domain with polygonal boundary Γ, $\psi : \mathbb{R} \to \mathbb{R}$ with $\psi(x) = (1 - x^2)^2/4$ and $\phi(x) = \psi'(x)$. We consider the Cahn-Hilliard

problem: *Find* $u(x,t) : \Omega \times [0,T] \to \mathbb{R}$ *such that:*

$$\dot{u} - \Delta\big(\phi(u) - \gamma^2 \Delta u\big) = 0 \qquad \text{in } \Omega \times [0,T], \tag{10.1a}$$

$$u(\cdot,0) = u_0(\cdot) \qquad \text{in } \Omega, \tag{10.1b}$$

$$\partial_n u = \partial_n\big(\phi(u) - \gamma^2 \Delta u\big) = 0 \qquad \text{on } \partial\Omega \times [0,T], \tag{10.1c}$$

where ∂_n denotes the (outward) normal derivative and $\gamma \in \mathbb{R}^+$, $0 < \gamma \ll 1$, represents the interface parameter. On the domain boundary we impose a no flux-type condition on u and the chemical potential $\phi(u) - \gamma^2 \Delta u$.

To define the variational formulation of problem (10.1a)–(10.1c) we introduce the three bilinear forms:

$$a^{\Delta}(v,w) = \int_\Omega (\nabla^2 v) : (\nabla^2 w)\, d\mathbf{x} \qquad \forall v, w \in H^2(\Omega),$$

$$a^{\nabla}(v,w) = \int_\Omega \nabla v \cdot \nabla w\, d\mathbf{x} \qquad \forall v, w \in H^1(\Omega),$$

$$a^{0}(v,w) = \int_\Omega v\, w\, d\mathbf{x} \qquad \forall v, w \in L^2(\Omega),$$

(∇^2 being the Hessian operator) and the semi-linear form

$$r(z;v,w) = \int_\Omega \phi'(z) \nabla v \cdot \nabla w\, d\mathbf{x} \quad \forall z, v, w \in H^2(\Omega).$$

Finally, introducing the functional space

$$V = \big\{ v \in H^1(\Omega) \,:\, \partial_n v = 0 \text{ on } \Gamma \big\}, \tag{10.2}$$

which is a subspace of $H^1(\Omega)$.

The weak formulation of problem (10.1a)–(10.1c) reads as: *Find* $u(\cdot,t) \in V$ *such that*

$$a^0(\dot{u}, v) + \gamma^2 a^{\Delta}(u,v) + r(u;u,v) = 0 \quad \forall v \in V, \tag{10.3a}$$

$$u(\cdot,0) = u_0. \tag{10.3b}$$

10.3.2 The Conforming Virtual Element Approximation

In this section, we introduce the main building blocks for the conforming virtual discretization of the Cahn-Hilliard equation, report a convergence result and collect some numerical results assessing the theoretical properties of the proposed scheme.

10.3.2.1 A C^1 Virtual Element Space

We briefly recall the construction of the virtual element space $W_h \subset H^2(\Omega)$ that we use to discretize (10.3a)–(10.3b); see [6] for more details.

Given an element $\mathsf{P} \in \Omega_h$, the *augmented* local space $\widetilde{V}_{h|\mathsf{P}}$ is defined by

$$\widetilde{V}_{h|\mathsf{P}} = \Big\{ v \in H^2(\mathsf{P}) \ : \Delta^2 v \in \mathbb{P}_2(\mathsf{P}),\, v_{|\partial\mathsf{P}} \in C^0(\partial\mathsf{P}),\, v_{|\mathsf{e}} \in \mathbb{P}_3(\mathsf{e}) \quad \forall \mathsf{e} \in \partial\mathsf{P}, \\ \nabla v_{|\partial\mathsf{P}} \in \big[C^0(\partial\mathsf{P})\big]^2,\, \partial_n v_{|\mathsf{e}} \in \mathbb{P}_1(\mathsf{e}) \quad \forall \mathsf{e} \in \partial\mathsf{P} \Big\}, \tag{10.4}$$

with ∂_n denoting the (outward) normal derivative.

Remark 10.1 The space $\widetilde{V}_{h|\mathsf{P}}$ corresponds to the space $\tilde{V}^p_{h,2p-1}(\mathsf{P})$ with $p = 2$ introduced in Sect. 10.2.2.2.

We consider the two sets of linear operators from $\widetilde{V}_{h|\mathsf{P}}$ into $\mathbb{R}$ denoted by **(D1)** and **(D2)** and defined as follows:

(D1) contains linear operators evaluating v_h at the $n = n(\mathsf{P})$ vertices of P;
(D2) contains linear operators evaluating ∇v_h at the $n = n(\mathsf{P})$ vertices of P.

The output values of the two sets of operators **(D1)** and **(D2)** are sufficient to uniquely determine v_h and ∇v_h on the boundary of P (cf. Sect. 10.2.2.2).

We use of the following local bilinear forms for all $\mathsf{P} \in \Omega_h$

$$a^{\Delta}_{\mathsf{P}}(v, w) = \int_{\mathsf{P}} (\nabla^2 v) : (\nabla^2 w)\, d\mathbf{x} \quad \forall v, w \in H^2(\mathsf{P}), \tag{10.5}$$

$$a^{\nabla}_{\mathsf{P}}(v, w) = \int_{\mathsf{P}} \nabla v \cdot \nabla w\, d\mathbf{x} \quad \forall v, w \in H^1(\mathsf{P}), \tag{10.6}$$

$$a^{0}_{\mathsf{P}}(v, w) = \int_{\mathsf{P}} v\, w\, d\mathbf{x} \qquad \forall v, w \in L^2(\mathsf{P}). \tag{10.7}$$

Now, we introduce the elliptic projection operator $\Pi_2^{\Delta,\mathsf{P}} : \widetilde{V}_{h|\mathsf{P}} \to \mathbb{P}_2(\mathsf{P})$ defined by

$$a^{\Delta}_{\mathsf{P}}(\Pi_2^{\Delta,\mathsf{P}} v_h, q) = a^{\Delta}_{\mathsf{P}}(v_h, q) \qquad \forall q \in \mathbb{P}_2(\mathsf{P}), \tag{10.8}$$

$$(\!(\Pi_2^{\Delta,\mathsf{P}} v_h, q)\!)_{\mathsf{P}} = (\!(v_h, q)\!)_{\mathsf{P}} \qquad \forall q \in \mathbb{P}_1(\mathsf{P}), \tag{10.9}$$

for all $v_h \in \widetilde{V}_{h|\mathsf{P}}$ where $(\!(\cdot,\cdot)\!)_{\mathsf{P}}$ is the Euclidean scalar product acting on the vectors that collect the vertex function values, i.e.

$$(\!(v_h, w_h)\!)_{\mathsf{P}} = \sum_{\mathsf{v} \in \mathscr{V}_{\mathsf{P}}} v_h(\mathsf{v})\, w_h(\mathsf{v}) \quad \forall v_h, w_h \in C^0(\mathsf{P}).$$

As shown in [6], the operator $\Pi_2^{\Delta,\mathsf{P}} : \widetilde{V}_{h|\mathsf{P}} \to \mathbb{P}_2(\mathsf{P})$ is well defined and uniquely determined on the basis of the informations carried by the linear operators in **(D1)** and **(D2)**.

Hinging upon the augmented space $\widetilde{V}_{h|\mathsf{P}}$ and employing the projector $\Pi_2^{\Delta,\mathsf{P}}$ we define our virtual local space

$$W_{h|\mathsf{P}} = \left\{ v \in \widetilde{V}_{h|\mathsf{P}} \, : \, a^0_{\mathsf{P}}(\Pi_2^{\Delta,\mathsf{P}}(v), q) = a^0_{\mathsf{P}}(v, q) \quad \forall q \in \mathbb{P}_2(\mathsf{P}) \right\}. \tag{10.10}$$

Since $W_{h|\mathsf{P}} \subset \widetilde{V}_{h|\mathsf{P}}$, operator $\Pi_2^{\Delta,\mathsf{P}}$ is well defined on $W_{h|\mathsf{P}}$ and computable by using the values provided by **(D1)** and **(D2)**. Moreover, the set of operators **(D1)** and **(D2)** constitutes a set of degrees of freedom for the space $W_{h|\mathsf{P}}$. Finally, there holds $\mathbb{P}_2(\mathsf{P}) \subseteq W_{h|\mathsf{P}}$.

We now introduce two further projectors on the local space $W_{h|\mathsf{P}}$, namely $\Pi_2^{0,\mathsf{P}}$ and $\Pi_2^{\nabla,\mathsf{P}}$, that will be employed together with the above projector $\Pi_2^{\Delta,\mathsf{P}}$ to build the discrete counterparts of the bilinear forms in (10.5). Operator $\Pi_2^{0,\mathsf{P}} : W_{h|\mathsf{P}} \to \mathbb{P}_2(\mathsf{P})$ is the standard L^2 projector on the space of quadratic polynomials in P. This is computable by means of the values of the degrees of freedom **(D1)** and **(D2)** (cf. [6]). To define $\Pi_2^{\nabla,\mathsf{P}} : W_{h|\mathsf{P}} \to \mathbb{P}_2(\mathsf{P})$ we need the additional bilinear form $a^{\nabla}(\cdot,\cdot) : W_{h|\mathsf{P}} \times W_{h|\mathsf{P}} \to \mathbb{R}$ that is given by

$$a^{\nabla}(v, w) = \int_{\Omega} \nabla v \cdot \nabla w \, d\mathbf{x} \quad \forall v, w \in H^1(\Omega).$$

Operator $\Pi_2^{\nabla,\mathsf{P}}$ is the elliptic projection defined with respect to $a^{\nabla}(\cdot,\cdot)$:

$$a^{\nabla}_{\mathsf{P}}(\Pi_2^{\nabla,\mathsf{P}} v_h, q) = a^{\nabla}_{\mathsf{P}}(v_h, q) \quad \forall q \in \mathbb{P}_2(\mathsf{P}), \tag{10.11a}$$

$$\int_{\mathsf{P}} \Pi_2^{\nabla,\mathsf{P}} v_h d\mathbf{x} = \int_{\mathsf{P}} v_h \, d\mathbf{x}. \tag{10.11b}$$

Such operator is well defined and uniquely determined by the values of **(D1)** and **(D2)** [6].

We are now ready to introduce the global virtual element space, which defined as follows

$$W_h = \left\{ v \in V \, : \, v_{|\mathsf{P}} \in W_{h|\mathsf{P}} \quad \forall \mathsf{P} \in \Omega_h \right\}.$$

The virtual element functions in W_h and their gradients are continuous fields on Ω, so this functional space is a conforming subspace of $H^2(\Omega)$. The *global degrees of freedom* of W_h are obtained by collecting the elemental degrees of freedom, so the

dimension of W_h is three times the number of the mesh vertices, and every virtual element function v_h defined on Ω is uniquely determined by

(i) its values at the mesh vertices;
(ii) its gradient values at the mesh vertices.

Finally, we recommended to scale the degrees of freedom **(D2)** by some local characteristic mesh size h_{V} in order to obtain a better condition number of the final system.

10.3.2.2 Virtual Element Bilinear Forms

We start by introducing the discrete versions of the elemental bilinear form forms in (10.5). Let $\mathsf{P} \in \Omega_h$ be a generic mesh element and $s_{\mathsf{P}}(\cdot,\cdot) : W_{h|\mathsf{P}} \times W_{h|\mathsf{P}} \to \mathbb{R}$ the positive definite bilinear form given by:

$$s_{\mathsf{P}}(v_h, w_h) = \sum_{\mathsf{V} \in \mathscr{V}_{\mathsf{P}}} \Big(v_h(\mathsf{V})\, w_h(v) + h_{\mathsf{V}}^2\, \nabla v_h(\mathsf{V}) \cdot \nabla w_h(\mathsf{V}) \Big) \quad \forall v_h, w_h \in W_{h|\mathsf{P}},$$

where h_{V} is a characteristic mesh size lenght associated with node V, e.g., the maximum diameter among the elements having V as a vertex.

Recalling (10.5), we consider the virtual element bilinear forms:

$$a^{\Delta}_{h,\mathsf{P}}(v_h, w_h) = a^{\Delta}_{\mathsf{P}}(\Pi_2^{\Delta,\mathsf{P}} v_h, \Pi_2^{\Delta,\mathsf{P}} w_h) + h_{\mathsf{P}}^{-2} s_{\mathsf{P}}\big(v_h - \Pi_2^{\Delta,\mathsf{P}} v_h, w_h - \Pi_2^{\Delta,\mathsf{P}} w_h\big), \tag{10.12}$$

$$a^{\nabla}_{h,\mathsf{P}}(v_h, w_h) = a^{\nabla}_{\mathsf{P}}(\Pi_2^{\nabla,\mathsf{P}} v_h, \Pi_2^{\nabla,\mathsf{P}} w_h) + s_{\mathsf{P}}\big(v_h - \Pi_2^{\nabla,\mathsf{P}} v_h, w_h - \Pi_2^{\nabla,\mathsf{P}} w_h\big), \tag{10.13}$$

$$a^{0}_{h,\mathsf{P}}(v_h, w_h) = a^{0}_{\mathsf{P}}(\Pi_2^{0,\mathsf{P}} v_h, \Pi_2^{0,\mathsf{P}} w_h) + h_{\mathsf{P}}^{2} s_{\mathsf{P}}\big(v_h - \Pi_2^{0,\mathsf{P}} v_h, w_h - \Pi_2^{0,\mathsf{P}} w_h\big) \tag{10.14}$$

for all $v_h, w_h \in W_{h|\mathsf{P}}$. Under the mesh regularity conditions of Sect. 10.1.3, we can prove the consistency and stability of the discrete bilinear forms. Let the symbol $\dagger$ stands for "Δ", "∇" or "0". We have:

(A) *(polynomial consistency)* $a^{\dagger}_{h,\mathsf{P}}(p, v_h) = a^{\dagger}_{\mathsf{P}}(p, v_h) \quad \forall p \in \mathbb{P}_2(\mathsf{P}),\ v_h \in W_{h|\mathsf{P}}$;

(B) *(stability)* there exist two positive constants c_* and c^* independent of h and the element $\mathsf{P} \in \Omega_h$ such that

$$c_* a^{\dagger}_{\mathsf{P}}(v_h, v_h) \le a^{\dagger}_{h,\mathsf{P}}(v_h, v_h) \le c^* a^{\dagger}_{\mathsf{P}}(v_h, v_h) \quad \forall v_h \in W_{h|\mathsf{P}}.$$

A consequence of the above properties is that the bilinear form $a^{\dagger}_{h,\mathsf{P}}(\cdot,\cdot)$ is continuous with respect to the relevant norm, which is H^2 for (10.12), H^1 for (10.13), and L^2 for (10.14). For every choice of †, the corresponding global bilinear form is

$$a^{\dagger}_h(v_h, w_h) = \sum_{\mathsf{P}\in\Omega_h} a^{\dagger}_{h,\mathsf{P}}(v_h, w_h) \quad \forall v_h, w_h \in W_h.$$

(10.1a)–(10.1c)

We now turn our attention to the semilinear form $r(\cdot;\cdot,\cdot)$, which we can also write as the sum of elemental contributions:

$$r(z; v, w) = \sum_{\mathsf{P}\in\Omega_h} r_{\mathsf{P}}(z; v, w) \quad \forall z, vw \in H^2(\Omega)$$

where

$$r_{\mathsf{P}}(z; v, w) = \int_{\mathsf{P}} (3z^2 - 1)\nabla v \cdot \nabla w d\mathbf{x} \quad \forall \mathsf{P} \in \Omega_h.$$

On each element P, we approximate the term $z(x)^2$ by means of its cell average, which we compute using the $L^2(\mathsf{P})$ bilinear form $a^0_{h,\mathsf{P}}(\cdot,\cdot)$:

$$z^2_{h|\mathsf{P}} \approx |\mathsf{P}|^{-1}\, a^0_{h,\mathsf{P}}(z_h, z_h),$$

where we recall that $|\mathsf{P}|$ is the area of element P. This approach has the correct approximation properties and preserves the positivity of z^2.

We therefore propose the following approximation of the local nonlinear forms

$$r_{h,\mathsf{P}}(z_h; v_h, w_h) = \widehat{\phi'(z_h)}_{|\mathsf{P}}\, a^{\nabla}_{h,\mathsf{P}}(v_h, w_h) \quad \forall z_h, v_h, w_h \in W_{h|\mathsf{P}},$$

where $\widehat{\phi'(z_h)}_{|\mathsf{P}} = 3\,|\mathsf{P}|^{-1}\, a^0_{h,\mathsf{P}}(z_h, z_h) - 1$. The global form is then assembled as

$$r_h(z_h; v_h, w_h) = \sum_{\mathsf{P}\in\Omega_h} r_{h,\mathsf{P}}(z_h; v_h, w_h) \quad \forall z_h, v_h w_h \in W_h.$$

10.3.2.3 The Discrete Problem

The virtual element discretization of problem (10.3a), (10.3b) follows a Galerkin approach in space combined with a backward Euler time-stepping scheme. Consider

the functional space

$$W_h^0 = W_h \cap V = \left\{ v \in W_h \ : \ \partial_n v = 0 \text{ on } \partial\Omega \right\},$$

which includes the boundary conditions. Then, we introduce the semi-discrete approximation: *Find* $u_h(\cdot, t)$ in W_h^0 *such that*

$$a_h^0(\dot{u_h}, v_h) + \gamma^2 a_h^{\Delta}(u_h, v_h) + r_h(u_h; u_h, v_h) = 0 \quad \forall v_h \in W_h^0, \tag{10.15}$$

$$u_h(0, \cdot) = u_{0,h}(\cdot), \tag{10.16}$$

where $u_{0,h}$ is a suitable approximation of u_0 in W_h^0 and $a_h^0(\cdot, \cdot)$, a_h^{Δ} and r_h are the virtual element bilinear forms defined in the previous section.

To formulate the fully discrete scheme, we subdivide the time interval $[0, T]$ into N uniform sub-intervals of length $k = T/N$ by means of the time nodes $0 = {}_0 < {}_1 < \ldots < {}_{N-1} < {}_N = T$, and denote the virtual element approximation of the solution $u(\cdot,)$ at $u(\cdot, {}^i)$ in W_h^0 by $u_{h,k}^i$. The fully discrete problem reads as: *Given* $u_{hk}^0 = u_{0,h} \in W_h^0$, *find* $u_{hk}^i \in W_h^0$, $i = 1, \ldots, N$ *such that*

$$k^{-1} a_h^0(u_{hk}^i - u_{hk}^{i-1}, v_h) + \gamma^2 a_h^{\Delta}(u_{hk}^i, v_h) + r_h(u_{hk}^i, u_{hk}^i; v_h) = 0 \quad \forall v_h \in W_h^0. \tag{10.17}$$

The semidiscrete Virtual Element formulation given in (10.15)–(10.16) converges to the exact solution of problem (10.3a)–(10.3b) according to the result stated in this theorem and proved in [6].

Theorem 10.6 *Let* u *be the solution of problem* (10.3a)–(10.3b). *Let* u_h *be the virtual element approximation provided by* (10.15)–(10.16) *and assume that*

$$||u_h||_{L^\infty(\Omega)} \leq C$$

for all $t \in (0, T]$ *and some positive contant* C *independent of* h. *Then, it holds that*

$$||u - u_h||_{L^2(\Omega)} \lesssim h^2$$

for every $\in [0, T]$.

10.3.3 Numerical Results

In this test, taken from [6] we study the convergence of our VEM discretization applied to the Cahn-Hilliard problem with a load term f obtained by enforcing as exact solution $u(x, y, t) = t \cos(2\pi x) \cos(2\pi y)$. The parameter γ is set to $1/10$ and the time step size Δ is $1e-7$. The H^2, H^1 and L^2 errors are computed at $t = 0.1$

on four quadrilateral meshes discretizing the unit square. The time discretization is performed by the Backward Euler method. The resulting non-linear system (10.17) at each time step is solved by the Newton method, using the l^2 norm of the relative residual as a stopping criterion. The tolerance for convergence is $1e-6$.

The results reported in Table 10.1 show that the VEM method converges is convergent with a convergence rate close to 2 in the L^2 norm as expected from Theorem 10.6. In the H^2 and H^1 seminorms, the method converges with order 1 and 2 respectively, as we can expect from the FEM theory and the approximation properties of the virtual element space. Finally, in Fig. 10.2 we report the results of a spinoidal decomposition. For completeness, we recall that spinodal decomposition is a physical phenomenon consisting of the separation of a mixture of two or more components to bulk regions of each, which occurs when a high-temperature mixture of different components is rapidly cooled. We employ an initial datum u_0 chosen to be a uniformly distributed random perturbation between -1 and 1. Results are consistent with the literature, cf. [6].

Table 10.1 H^2, H^1 and L^2 errors and convergence rates α computed on four quadrilateral meshes discretizing the unit square [6]

h	$\lvert u-u_h\rvert_{H^2(\Omega)}$	α	$\lvert u-u_h\rvert_{H^1(\Omega)}$	α	$\lVert u-u_h\rVert_{L^2(\Omega)}$	α
1/16	1.35e−1	–	8.57e−2	–	8.65e−2	–
1/32	5.86e−2	1.20	2.20e−2	1.96	2.20e−2	1.97
1/64	2.79e−2	1.07	5.53e−3	1.99	5.52e−3	1.99
1/128	1.38e−2	1.02	1.37e−3	2.01	1.37e−3	2.01

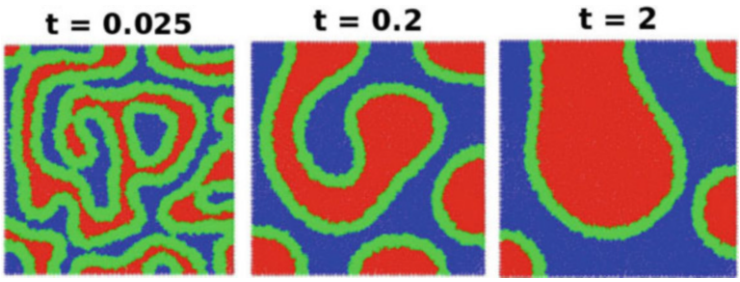

Fig. 10.2 Spinoidal decomposition on the unit square at three temporal frames for a Voronoi polygonal mesh of 4096 elements

10.4 The Virtual Element Method for the Elastodynamics Problem

10.4.1 The Continuous Problem

We consider an elastic body occupying the open, bounded polygonal domain $\Omega \subset \mathbb{R}^2$ with Lipschitz boundary Γ. We assume that boundary Γ can be split into the two disjoint subsets Γ_D and Γ_N, so that $\Gamma = \Gamma_D \cup \Gamma_N$ and with the one-dimensional Lebesgue measure (length) $|\Gamma_D \cap \Gamma_N| = 0$. For the well-posedness of the mathematical model, we further require length of Γ_D is nonzero, i.e., $|\Gamma_D| > 0$. Let $T > 0$ denote the final time. We consider the external load $\mathbf{f} \in L^2\big(0, T; [L^2(\Omega)]^2\big)$, the boundary function $\mathbf{g}_N \in C^1\big(0, T; [H^{1/2}_{0,\Gamma_N}]^2\big)$, and the initial functions $\mathbf{u}_0 \in [H^1_{0,\Gamma_D}(\Omega)]^2$, $\mathbf{u}_1 \in [L^2(\Omega)]^2$. For such time-dependent vector fields, we may indicate the dependence on time explicitly, e.g., $\mathbf{f}(t) := \mathbf{f}(\cdot, t) \in [L^2(\Omega)]^2$, or drop it out to ease the notation when it is obvious from the context.

The equations governing the two-dimensional initial/boundary-value problem of linear elastodynamics for the displacement vector $\mathbf{u} : \Omega \times [0, T] \to \mathbb{R}^2$ are:

$$\rho \ddot{\mathbf{u}} - \nabla \cdot \boldsymbol{\sigma}(\mathbf{u}) = \mathbf{f} \qquad \text{in } \Omega \times (0, T], \tag{10.1}$$

$$\mathbf{u} = \mathbf{0} \qquad \text{on } \Gamma_D \times (0, T], \tag{10.2}$$

$$\boldsymbol{\sigma}(\mathbf{u})\mathbf{n} = \mathbf{g}_N \qquad \text{on } \Gamma_N \times (0, T], \tag{10.3}$$

$$\mathbf{u} = \mathbf{u}_0 \qquad \text{in } \Omega \times \{0\}, \tag{10.4}$$

$$\dot{\mathbf{u}} = \mathbf{u}_1 \qquad \text{in } \Omega \times \{0\}. \tag{10.5}$$

Here, ρ is the mass density, which we suppose to be a strictly positive and uniformly bounded function and $\boldsymbol{\sigma}(\mathbf{u})$ is the stress tensor. In (10.2) we assume homogeneous Dirichlet boundary conditions on Γ_D. This assumption is made only to ease the exposition and the analysis, as our numerical method is easily extendable to nonhomogeneous Dirichlet boundary conditions.

We denote the space of the symmetric, 2×2-sized, real-valued tensors by $\mathbb{R}^{2\times 2}_{\text{sym}}$ and assume that the stress tensor $\boldsymbol{\sigma} : \Omega \times [0, T] \to \mathbb{R}^{2\times 2}_{\text{sym}}$ is expressed, according to Hooke's law, by $\boldsymbol{\sigma}(\mathbf{u}) = \mathscr{D}\boldsymbol{\varepsilon}(\mathbf{u})$, where, $\boldsymbol{\varepsilon}(\mathbf{u})$ denotes the symmetric gradient of $\mathbf{u}$, i.e., $\boldsymbol{\varepsilon}(\mathbf{u}) = \big(\nabla\mathbf{u} + (\nabla\mathbf{u})^T\big)/2$, and $\mathscr{D} = \mathscr{D}(\mathbf{x}) : \mathbb{R}^{2\times 2}_{\text{sym}} \longrightarrow \mathbb{R}^{2\times 2}_{\text{sym}}$ is the *stiffness* tensor

$$\mathscr{D}\boldsymbol{\tau} = 2\mu\boldsymbol{\tau} + \lambda \text{tr}(\boldsymbol{\tau})\mathsf{I} \tag{10.6}$$

for all $\boldsymbol{\tau} \in \mathbb{R}^{2\times 2}_{\text{sym}}$. In this definition, I and $\text{tr}(\cdot)$ are the identity matrix and the trace operator; λ and μ are the first and second Lamé coefficients, which we assume to

be in $L^\infty(\Omega)$ and nonnegative. The compressional (P) and shear (S) wave velocities of the medium are respectively obtained through the relations $c_P = \sqrt{(\lambda + 2\mu)/\rho}$ and $c_S = \sqrt{\mu/\rho}$.

Let $\mathbf{V} = \left[H^1_{\Gamma_D}(\Omega)\right]^2$ be the space of H^1 vector-valued functions with null trace on Γ_D. We consider the two bilinear forms $m(\cdot,\cdot),\ a(\cdot,\cdot) : \mathbf{V} \times \mathbf{V} \to \mathbb{R}$ defined as

$$m(\mathbf{w}, \mathbf{v}) = \int_\Omega \rho \mathbf{w} \cdot \mathbf{v}\, d\mathbf{x} \quad \forall \mathbf{w},\ \mathbf{v} \in \mathbf{V}, \tag{10.7}$$

$$a(\mathbf{w}, \mathbf{v}) = \int_\Omega \boldsymbol{\sigma}(\mathbf{w}) : \boldsymbol{\varepsilon}(\mathbf{v})\, d\mathbf{x} \quad \forall \mathbf{w},\ \mathbf{v} \in \mathbf{V}, \tag{10.8}$$

and the linear functional $F(\cdot) : \mathbf{V} \to \mathbb{R}$ defined as

$$F(\mathbf{v}) = \int_\Omega \mathbf{f} \cdot \mathbf{v}\, d\mathbf{x} + \int_{\Gamma_N} \mathbf{g}_N \cdot \mathbf{v}\, ds \quad \forall \mathbf{v} \in \mathbf{V}. \tag{10.9}$$

The variational formulation of the linear elastodynamics equations reads as: *For all* $t \in (0, T]$ *find* $\mathbf{u}(t) \in \mathbf{V}$ *such that for* $t = 0$ *it holds that* $\mathbf{u}(0) = \mathbf{u}_0$ *and* $\dot{\mathbf{u}}(0) = \mathbf{u}_1$ *and*

$$m(\ddot{\mathbf{u}}, \mathbf{v}) + a(\mathbf{u}, \mathbf{v}) = F(\mathbf{v}) \qquad \forall \mathbf{v} \in \mathbf{V}. \tag{10.10}$$

As shown, for example, by Raviart and Thomas (see Theorem 8–3.1 [90]) the variational problem (10.10) is well posed and its unique solution satisfies $\mathbf{u} \in C^0\big(0, T; \mathbf{V}\big) \cap C^1\big(0, T; [L^2(\Omega)]^2\big)$.

10.4.2 The Conforming Virtual Element Approximation

In this section we introduce the main building blocks for the conforming virtual element discretization of the elastodynamics equation, report stability and convergence results and collect some numerical results assessing the theoretical properties of the proposed scheme.

10.4.2.1 Virtual Element Spaces

Let $k \geq 1$ be an integer number. The global virtual element space is defined as

$$\mathbf{V}_k^h := \left\{ \mathbf{v} \in \mathbf{V} \ :\ \mathbf{v}_{|\mathsf{P}} \in \mathbf{V}_k^h(\mathsf{P}) \text{ for every } \mathsf{P} \in \Omega_h \right\} \tag{10.11}$$

where $\mathbf{V}_k^h(\mathsf{P}) = \left[V_k^h(\mathsf{P})\right]^2$, with

$$V_k^h(\mathsf{P}) := \Big\{ v_h \in H^1(\mathsf{P}) \,:\, v_{h|_{\partial\mathsf{P}}} \in C(\partial\mathsf{P}),\ v_{h|_\mathsf{e}} \in \mathbb{P}_k(\mathsf{e})\ \forall \mathsf{e} \in \partial\mathsf{P},\ \Delta v_h \in \mathbb{P}_k(\mathsf{P}),$$
$$\big(v_h - \Pi_k^\nabla v_h, \mu_h\big)_\mathsf{P} = 0\ \forall \mu_h \in \mathbb{P}_k(\mathsf{P})\backslash\mathbb{P}_{k-2}(\mathsf{P}) \Big\}, \tag{10.12}$$

where $\Pi_k^\nabla : H^1(\mathsf{P}) \cap C^0(\overline{\mathsf{P}}) \to \mathbb{P}_k(\mathsf{P})$ is the usual elliptic projection of a function v_h on the space of polynomials of degree k, cf. (10.11)–(10.12).

Each virtual element function $v_h \in V_k^h(\mathsf{P})$ is uniquely characterized by

(C1) the values of v_h at the vertices of P;
(C2) the moments of v_h of order up to $k-2$ on each one-dimensional edge $\mathsf{e} \in \partial\mathsf{P}$:

$$\frac{1}{|\mathsf{e}|}\int_\mathsf{e} v_h\, m\, ds,\ \forall m \in \mathscr{M}_{k-2}(\mathsf{e}),\ \forall \mathsf{e} \in \partial\mathsf{P}; \tag{10.13}$$

(C3) the moments of v_h of order up to $k-2$ on P:

$$\frac{1}{|\mathsf{P}|}\int_\mathsf{P} v_h\, m\, d\mathbf{x},\ \forall m \in \mathscr{M}_{k-2}(\mathsf{P}). \tag{10.14}$$

As usual, the degrees of freedom of the global space $\mathbf{V}_k^h$ are provided by collecting all the local degrees of freedom (which allow the computation of the elliptic projection Π_k^∇), and their unisolvence is an immediate consequence of the unisolvence of the local degrees of freedom for the elemental spaces $V_k^h(\mathsf{P})$.

10.4.2.2 Discrete Bilinear Forms

In the virtual element setting, we define the bilinear forms $m_h(\cdot,\cdot)$ and $a_h(\cdot,\cdot)$ as the sum of elemental contributions, which are respectively denoted by $m_{h,\mathsf{P}}(\cdot,\cdot)$ and $a_{h,\mathsf{P}}(\cdot,\cdot)$:

$$m_h(\cdot,\cdot) : \mathbf{V}_k^h \times \mathbf{V}_k^h \to \mathbb{R}, \quad \text{with} \quad m_h(\mathbf{v}_h, \mathbf{w}_h) = \sum_{\mathsf{P}\in\Omega_h} m_{h,\mathsf{P}}(\mathbf{v}_h, \mathbf{w}_h),$$

$$a_h(\cdot,\cdot) : \mathbf{V}_k^h \times \mathbf{V}_k^h \to \mathbb{R}, \quad \text{with} \quad a_h(\mathbf{v}_h, \mathbf{w}_h) = \sum_{\mathsf{P}\in\Omega_h} a_{h,\mathsf{P}}(\mathbf{v}_h, \mathbf{w}_h).$$

The local bilinear form $m_{h,\mathsf{P}}(\cdot,\cdot)$ is given by

$$m_{h,\mathsf{P}}(\mathbf{v}_h, \mathbf{w}_h) = \int_\mathsf{P} \rho\, \Pi_k^0 \mathbf{v}_h \cdot \Pi_k^0 \mathbf{w}_h\, dV + S_m^\mathsf{P}(\mathbf{v}_h, \mathbf{w}_h), \tag{10.15}$$

where $S_m^{\mathsf{P}}(\cdot,\cdot)$ is the local stabilization term. The bilinear form $m_{h,\mathsf{P}}$ depends on the orthogonal projections $\Pi_k^0\mathbf{v}_h$ and $\Pi_k^0\mathbf{w}_h$, which are computable from the degrees of freedom of $\mathbf{v}_h$ and $\mathbf{w}_h$. The local form $S_m^{\mathsf{P}}(\cdot,\cdot) : \mathbf{V}_k^h \times \mathbf{V}_k^h \to \mathbb{R}$ can be *any* symmetric and coercive bilinear form that is computable from the degrees of freedom and for which there exist two strictly positive real constants σ_* and σ^* such that

$$\sigma_* m_{\mathsf{P}}(\mathbf{v}_h,\mathbf{v}_h) \leq S_m^{\mathsf{P}}(\mathbf{v}_h,\mathbf{v}_h) \leq \sigma^* m_{\mathsf{P}}(\mathbf{v}_h,\mathbf{v}_h) \quad \mathbf{v}_h \in \ker\left(\Pi_k^0\right) \cap \mathbf{V}_k^h(\mathsf{P}). \tag{10.16}$$

Computable stabilizations $S_m^{\mathsf{P}}(\cdot,\cdot)$ are provided by resorting to the two-dimensional stabilizations of the effective choices for the scalar case proposed in the literature [54, 79].

The local bilinear form $a_{h,\mathsf{P}}$ is given by

$$a_{h,\mathsf{P}}(\mathbf{v}_h,\mathbf{w}_h) = \int_{\mathsf{P}} \mathbf{D}\Pi_{k-1}^0(\boldsymbol{\varepsilon}(\mathbf{v}_h)) : \Pi_{k-1}^0(\boldsymbol{\varepsilon}(\mathbf{w}_h))\, dV + S_a^{\mathsf{P}}(\mathbf{v}_h,\mathbf{w}_h), \tag{10.17}$$

where $S_a^{\mathsf{P}}(\cdot,\cdot)$ is the local stabilization term. The bilinear form $a_{h,\mathsf{P}}$ depends on the orthogonal projections $\Pi_{k-1}^0\nabla\mathbf{v}_h$ and $\Pi_{k-1}^0\nabla\mathbf{w}_h$, which are computable from the degrees of freedom of $\mathbf{v}_h$ and $\mathbf{w}_h$. On its turn, $S_a^{\mathsf{P}}(\cdot,\cdot) : \mathbf{V}_k^h \times \mathbf{V}_k^h \to \mathbb{R}$ can be *any* symmetric and coercive bilinear form that is computable from the degrees of freedom and for which there exist two strictly positive real constants $\overline{\sigma}_*$ and $\overline{\sigma}^*$ such that

$$\overline{\sigma}_* a_{\mathsf{P}}(\mathbf{v}_h,\mathbf{v}_h) \leq S_m^{\mathsf{P}}(\mathbf{v}_h,\mathbf{v}_h) \leq \overline{\sigma}^* a_{\mathsf{P}}(\mathbf{v}_h,\mathbf{v}_h) \quad \mathbf{v}_h \in \ker\left(\Pi_k^0\right) \cap \mathbf{V}_k^h(\mathsf{P}). \tag{10.18}$$

Moreover, the bilinear form $S_a^{\mathsf{P}}(\cdot,\cdot)$ must scale with respect to h like $a_{\mathsf{P}}(\cdot,\cdot)$, i.e., as $\mathscr{O}(1)$. As before, we can define computable stabilizations $S_a^{\mathsf{P}}(\cdot,\cdot)$ by resorting to the two-dimensional stabilizations for the scalar case proposed in the literature [54, 79]. As usual, the discrete bilinear forms $a_{h,\mathsf{P}}(\cdot,\cdot)$ and $m_{h,\mathsf{P}}(\cdot,\cdot)$ satisfy the *k-consistency* and *stability* properties. The stability constants may depend on physical parameters and the polynomial degree k [11, 24].

10.4.2.3 Discrete Load Term

We approximate the right-hand side (10.21) of the variational formulation by means of the linear functional $F_h(\cdot) : \mathbf{V}_k^h \to \mathbb{R}^2$ given by

$$F_h(\mathbf{v}_h) = \int_\Omega \mathbf{f}\cdot\Pi_{k-2}^0(\mathbf{v}_h)\, dV + \sum_{\mathsf{e}\in\Gamma_N}\int_{\mathsf{e}} \mathbf{g}_N\cdot\mathbf{v}_h\, ds \quad \forall\mathbf{v}_h \in \mathbf{V}_k^h. \tag{10.19}$$

The linear functional $F_h(\cdot)$ is clearly computable since the edge trace $\mathbf{v}_{h|\mathrm{e}}$ is a known polynomial and $\Pi^0_k(\mathbf{v}_h)$ is computable from the degrees of freedom of $\mathbf{v}_h$. Moreover, $F_h(\cdot)$ is a bounded functional. In fact, when $\mathbf{g}_N = 0$ using the stability of the projection operator and the Cauchy-Schwarz inequality, we note that

$$|F_h(\mathbf{v}_h)| \leq \left| \int_\Omega \mathbf{f}(t) \cdot \Pi^0_{k-2}(\mathbf{v}_h)\, dV \right| \leq \|\mathbf{f}(t)\|_0 \left\| \Pi^0_{k-2}(\mathbf{v}_h) \right\|_0$$

$$\leq \|\mathbf{f}(t)\|_0 \, \|\mathbf{v}_h\|_0 \quad \forall t \in [0, T]. \tag{10.20}$$

This estimate is used in the proof of the stability of the semi-discrete virtual element approximation (see Theorem 10.7).

10.4.2.4 The Discrete Problem

The semi-discrete virtual element approximation of (10.10) reads as: *For all* $t \in (0, T]$ *find* $\mathbf{u}_h(t) \in \mathbf{V}^h_k$ *such that for* $t = 0$ *it holds that* $\mathbf{u}_h(0) = (\mathbf{u}_0)_I$ *and* $\dot{\mathbf{u}}_h(0) = (\mathbf{u}_1)_I$ *and*

$$m_h(\ddot{\mathbf{u}}_h, \mathbf{v}_h) + a_h(\mathbf{u}_h, \mathbf{v}_h) = F_h(\mathbf{v}_h) \quad \forall \mathbf{v}_h \in \mathbf{V}^h_k. \tag{10.21}$$

Here, $\mathbf{u}_h(t)$ is the virtual element approximation of $\mathbf{u}$ and $\mathbf{v}_h$ is the generic test function in $\mathbf{V}^h_k$, while $(\mathbf{u}_0)_I$ and $(\mathbf{u}_1)_I$ are the virtual element interpolants of the initial solution functions $\mathbf{u}(0)$ and $\dot{\mathbf{u}}(0)$.

We carry out the time integration by applying the leap-frog time marching scheme [89] to the second derivative in time $\ddot{\mathbf{u}}_h$. To this end, we subdivide the interval $(0, T]$ into N_T subintervals of amplitude $\Delta t = T/N_T$ and at every time level $t^n = n\Delta t$ we consider the variational problem for $n \geq 1$:

$$m_h(\mathbf{u}^{n+1}_h, \mathbf{v}_h) - 2m_h(\mathbf{u}^n_h, \mathbf{v}_h) + m_h(\mathbf{u}^{n-1}_h, \mathbf{v}_h) + \Delta t^2 a_h(\mathbf{u}^n_h, \mathbf{v}_h)$$

$$= \Delta t^2 F^n_h(\mathbf{v}_h) \quad \forall \mathbf{v}_h \in \mathbf{V}^h_k, \tag{10.22}$$

and initial step

$$m_h(\mathbf{u}^1_h, \mathbf{v}_h) - m_h(\mathbf{u}_0, \mathbf{v}_h) - \Delta t m_h(\mathbf{u}_1, \mathbf{v}_h) + \frac{\Delta t^2}{2} a_h(\mathbf{u}_0, \mathbf{v}_h)$$

$$= \frac{\Delta t^2}{2} F^0_h(\mathbf{v}_h) \quad \forall \mathbf{v}_h \in V^h_k.$$

The leap-frog scheme is second-order accurate, explicit and conditionally stable. [89] It is straightforward to show that these properties are inherited by the fully-discrete scheme (10.22).

10.4.2.5 Stability and Convergence Analysis for the Semi-Discrete Problem

We employ the *energy* norm

$$|||\mathbf{v}_h(t)|||^2 = \left|\left|\rho^{\frac{1}{2}}\dot{\mathbf{v}}_h(t)\right|\right|_0^2 + |\mathbf{v}_h(t)|_1^2, \qquad t \in [0,T], \tag{10.23}$$

which is defined for all $\mathbf{v}_h \in \mathbf{V}_k^h$. The local stability property of the bilinear forms $m_h(\cdot,\cdot)$ and $a_h(\cdot,\cdot)$ implies the equivalence relation

$$m_h(\dot{\mathbf{v}}_h,\dot{\mathbf{v}}_h) + a_h(\mathbf{v}_h,\mathbf{v}_h) \lesssim |||\mathbf{v}_h(t)|||^2 \lesssim m_h(\dot{\mathbf{v}}_h,\dot{\mathbf{v}}_h) + a_h(\mathbf{v}_h,\mathbf{v}_h) \tag{10.24}$$

for all time-dependent virtual element functions $\mathbf{v}_h(t)$ with square integrable derivative $\dot{\mathbf{v}}_h(t)$.

The hidden constants in (10.24) are independent of the mesh size parameter h [11]. However, they may depend on the stability parameters, the physical parameters and the polynomial degree k [25]. It is worth noting that the dependence on k does not seem to have a relevant impact on the optimality of the convergence rates in the numerical experiments of Sect. 10.4.3. The following stability result has been proved in [11].

Theorem 10.7 *Let* $\mathbf{f} \in L^2\big(0,T;[L^2(\Omega)]^2\big)$ *and let* $\mathbf{u}_h \in C^2\big(0,T;\mathbf{V}_k^h\big)$ *be the solution of* (10.21)*. Then, it holds*

$$|||\mathbf{u}_h(t)||| \lesssim |||(\mathbf{u}_0)_I||| + \int_0^t ||\mathbf{f}(\tau)||_{0,\Omega}\, d\tau. \tag{10.25}$$

The hidden constant in $\lesssim$ *is independent of* h*, but may depend on the model parameters and approximation constants and the polynomial degree* k*.*

We point out that in the case of $\mathbf{f}$ null external force, i.e. $\mathbf{f} = \mathbf{0}$, the above bound reduces to

$$|||\mathbf{u}_h(t)||| \lesssim |||(\mathbf{u}_0)_I|||$$

that is the virtual element approximation is dissipative.

Now, we recall [11] the convergence of the semi-discrete virtual element approximation in the energy norm (10.23).

Theorem 10.8 *Let* $\mathbf{u} \in C^2\big(0,T;[H^{m+1}(\Omega)]^2\big)$*,* $m \in \mathbb{N}$*, be the exact solution of problem* (10.10)*. Let* $\mathbf{u}_h \in \mathbf{V}_k^h$ *be the solution of the semi-discrete problem* (10.21)*.*

For $\mathbf{f} \in L^2\big((0,T);\big[H^{m-1}(\Omega)\big]^2\big)$ *we have that*

$$\sup_{0<t\le T} |||\mathbf{u}(t)-\mathbf{u}_h(t)||| \lesssim \frac{h^\mu}{k^m} \sup_{0<t\le T}\Big(\|\dot{\mathbf{u}}(t)\|_{m+1}+\|\mathbf{u}(t)\|_{m+1}\Big)$$
$$+\int_0^T \left(\frac{h^{\mu+1}}{k^m}\big(\|\ddot{\mathbf{u}}(\tau)\|_{m+1}+\|\dot{\mathbf{u}}(\tau)\|_{m+1}\big)+\frac{h^\mu}{k^m}\big(\|\ddot{\mathbf{u}}(\tau)\|_{m+1}+\|\dot{\mathbf{u}}(\tau)\|_{m+1}\big)\right) d\tau$$
$$+\int_0^T h\Big\|(I-\Pi^0_{k-2})\mathbf{f}(\tau)\Big\|_0 d\tau, \tag{10.26}$$

where $\mu=\min(k,m)$. *The hidden constant in "*$\lesssim$*" is independent of* h, *but may depend on the model parameters and approximation constants, the polynomial degree* k, *and the final observation time* T.

Finally, we state the convergence result in the L^2 norm, whose proof is again found in [11].

Theorem 10.9 *Let* $\mathbf{u}$ *be the exact solution of problem* (10.10) *under the assumption that domain* Ω *is* H^2*-regular and* $\mathbf{u}_h \in \mathbf{V}_k^h$ *the solution of the virtual element method stated in* (10.21). *If* $\mathbf{u},\dot{\mathbf{u}},\ddot{\mathbf{u}} \in L^2\big(0,T;\big[H^{m+1}(\Omega)\cap H_0^1(\Omega)\big]^2\big)$, *with integer* $m\ge 0$, *then the following estimate holds for almost every* $t\in[0,T]$ *by setting* $\mu=\min(m,k)$*:*

$$\|\mathbf{u}(t)-\mathbf{u}_h(t)\|_0 \lesssim \|\mathbf{u}_h(0)-\mathbf{u}_0\|_0+\|\dot{\mathbf{u}}_h(0)-\mathbf{u}_1\|_0+\frac{h^{\mu+1}}{k^{m+1}}\Big(\|\ddot{\mathbf{u}}\|_{L^2(0,T;[H^{m+1}(\Omega)]^2)}$$
$$+\|\dot{\mathbf{u}}\|_{L^2(0,T;[H^{m+1}(\Omega)]^2)}+\|\mathbf{u}\|_{L^2(0,T;[H^{m+1}(\Omega)]^2)}\Big)$$
$$+\int_0^T \Big\|\big(1-\Pi^0_{k-2}\big)\mathbf{f}(\tau)\Big\|_0^2 d\tau. \tag{10.27}$$

The hidden constant in "$\lesssim$*" is independent of* h, *but may depend on the model parameters and approximation constants* ϱ, μ^*, *and the polynomial degree* k, *and the final observation time* T.

10.4.3 Numerical Results

In this section, we report from [11] a set of numerical results assessing the convergence properties of the virtual element discretization by using a manufactured solution on three different mesh families, each one possessing some special feature.

In particular, we let $\Omega=(0,1)^2$ for $t\in[0,T]$, $T=1$, and consider initial condition $\mathbf{u}_0$, boundary condition $\mathbf{g}$ and forcing term $\mathbf{f}$ determined from the exact

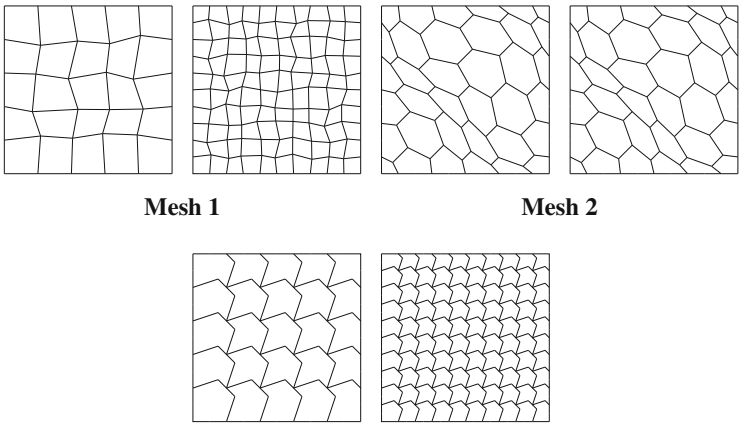

Fig. 10.3 Base meshes (top row) and first refined meshes (bottom row) of the following mesh families from left to right: randomized quadrilateral mesh; mainly hexagonal mesh; nonconvex octagonal mesh

solution:

$$\mathbf{u}(x, y, t) = \cos\left(\frac{2\pi\, t}{T}\right)\begin{pmatrix}\sin^2(\pi x)\sin(2\pi y)\\ \sin(2\pi x)\sin^2(\pi y)\end{pmatrix}. \tag{10.28}$$

To this end, we consider three different mesh partitionings, denoted by:

– *Mesh 1*, randomized quadrilateral mesh;
– *Mesh 2*, mainly hexagonal mesh with continuously distorted cells;
– *Mesh 3*, nonconvex octagonal mesh.

The base mesh and the first refined mesh of each mesh sequence are shown in Fig. 10.3.

The discretization in time is given by applying the leap-frog method with $\Delta t = 10^{-4}$ and carried out for 10^4 time cycles in order to reach time $T = 1$.

For these calculations, we used the VEM approximation based on the conforming space V_k^h with $k = 1, 2, 3, 4$ and the convergence curves for the three mesh sequences above are reported in Figs. 10.4, 10.5, and 10.6. The expected rate of convergence is shown in each panel by the triangle closed to the error curve and indicated by an explicit label. The results are in agreement with the theoretical estimates. To conclude, Fig. 10.7 shows the semilog error curves obtained through a"p"-type refinement calculation for the previous benchmark, i.e. for a fixed 5×5 mesh of type I the order of the virtual element space is increased from $k = 1$ to $k = 10$. We employ two different implementations, namely in the first case the space of polynomials of degree k is generated by the standard scaled monomials,

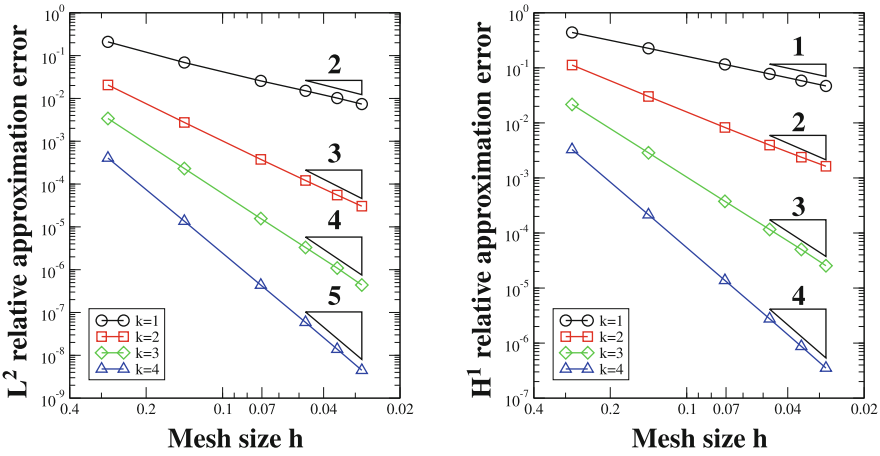

Fig. 10.4 Convergence plots for the virtual element approximation of Problem (10.1)–(10.5) with exact solution (10.28) using family *Mesh 1* of randomized quadrilateral meshes. Error curves are computed using the L^2 norm (left panels) and H^1 norm (right panels) and are plot versus h

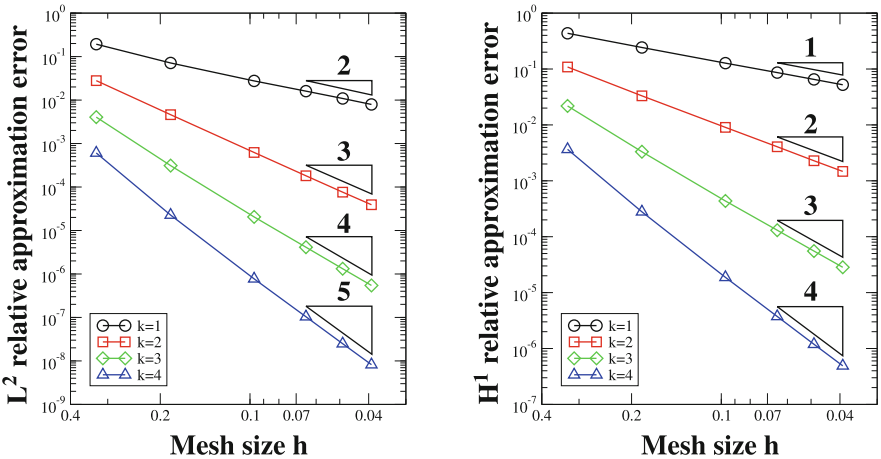

Fig. 10.5 Convergence plots for the virtual element approximation of Problem (10.1)–(10.5) with exact solution (10.28) using family *Mesh 2* of mainly hexagonal meshes. Error curves are computed using the L^2 norm (left panels) and H^1 norm (right panels) and are plotted versus h

while in the second one we consider an orthogonal polynomial basis. The behavior of the VEM when using nonorthogonal and orthogonal polynomial basis shown in Fig. 10.7 is in accordance with the literature, see, e.g., [31, 79].

Acknowledgments PFA and MV acknowledge the financial support of PRIN research grant number 201744KLJL "*Virtual Element Methods: Analysis and Applications*" funded by MIUR. PFA, IM, and MV, annd SS acknowledges the financial support of INdAM-GNCS. GM acknowledges the financial support of the ERC Project CHANGE, which has received funding from the European

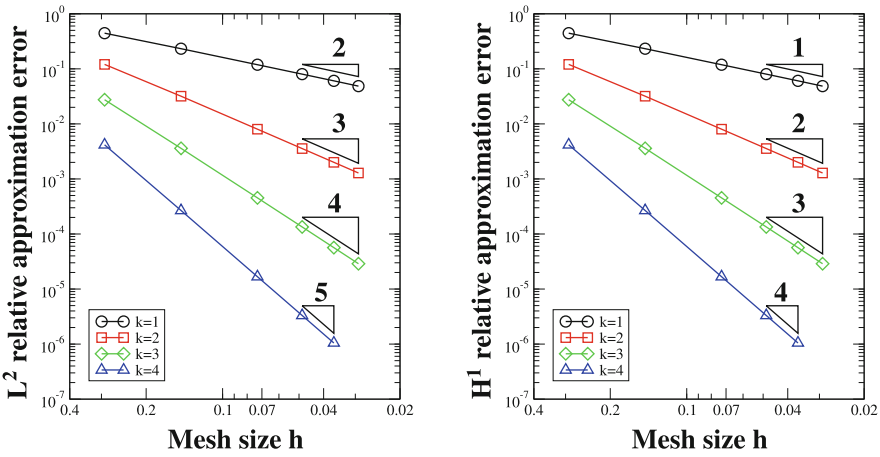

Fig. 10.6 Convergence plots for the virtual element approximation of Problem (10.1)–(10.5) with exact solution (10.28) using family *Mesh 3* of nonconvex octagonal meshes. Error curves are computed using the L^2 norm (left panels) and H^1 norm (right panels) and are plotted versus h

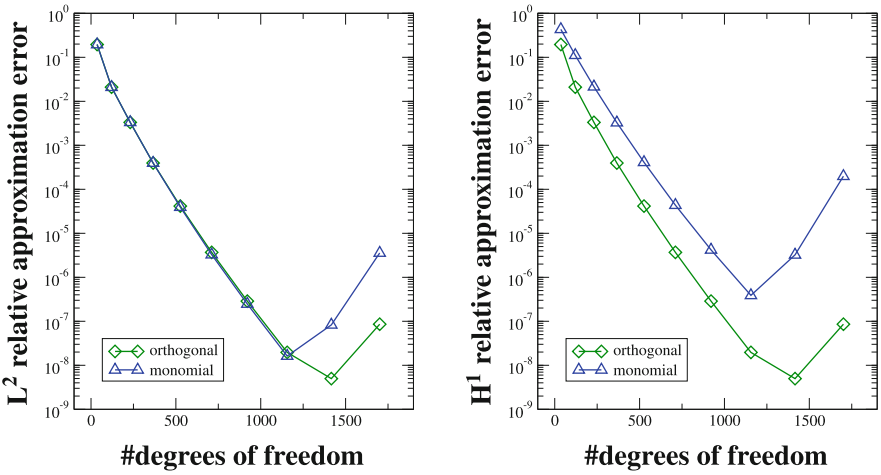

Fig. 10.7 Convergence plots for the virtual element approximation of Problem (10.1)–(10.5) with exact solution (10.28) using family *Mesh 1* of randomized quadrilateral meshes. Error curves are computed using k-refinement the L^2 norm (left panel) and H^1 norm (right panel) and are plot versus the number of degrees of freedom by performing a refinement of type "p" on a 5×5 mesh. Each plot shows the two convergence curves that are obtained using monomials (circles) and orthogonalized polynomials (squares)

Research Council under the European Union's Horizon 2020 research and innovation program (grant agreement no. 694515).

References

1. R.A. Adams, J.J.F. Fournier, in *Sobolev spaces*, 2 edn. Pure and Applied Mathematics (Academic Press, New York, 2003)
2. B. Ahmad, A. Alsaedi, F. Brezzi, L.D. Marini, A. Russo, Equivalent projectors for virtual element methods. Comput. Math. Appl. **66**(3), 376–391 (2013)
3. F. Aldakheel, B. Hudobivnik, A. Hussein, P. Wriggers, Phase-field modeling of brittle fracture using an efficient virtual element scheme. Comput. Methods Appl. Mech. Eng. **341**, 443–466 (2018)
4. P.F. Antonietti, I. Mazzieri, A. Quarteroni, F. Rapetti. Non-conforming high order approximations of the elastodynamics equation. Comput. Methods Appl. Mech. Eng. **209/212**, 212–238 (2012)
5. P.F. Antonietti, B. Ayuso de Dios, I. Mazzieri, A. Quarteroni, Stability analysis of discontinuous Galerkin approximations to the elastodynamics problem. J. Sci. Comput. **68**(1), 143–170 (2016)
6. P.F. Antonietti, L. Beirão da Veiga, S. Scacchi, M. Verani, A C^1 virtual element method for the Cahn-Hilliard equation with polygonal meshes. SIAM J. Numer. Anal. **54**(1), 34–56 (2016)
7. P.F. Antonietti, G. Manzini, M. Verani, The fully nonconforming virtual element method for biharmonic problems. Math. Models Methods Appl. Sci. **28**(2), 387–407 (2018)
8. P.F. Antonietti, I. Mazzieri, High-order discontinuous Galerkin methods for the elastodynamics equation on polygonal and polyhedral meshes. Comput. Methods Appl. Mech. Eng. **342**, 414–437 (2018)
9. P.F. Antonietti, G. Manzini, M. Verani, The conforming virtual element method for polyharmonic problems. Comput. Math. Appl. **79**(7), 2021–2034 (2020)
10. P.F. Antonietti, F. Bonaldi, I. Mazzieri, A high-order discontinuous Galerkin approach to the elasto-acoustic problem. Comput. Methods Appl. Mech. Eng. **358**, 112634, 29 (2020)
11. P.F. Antonietti, G. Manzini, I. Mazzieri, H.M. Mourad, M. Verani, The arbitrary-order virtual element method for linear elastodynamics models. convergence, stability and dispersion-dissipation analysis. Int. J. Numer. Methods Eng. **122**(4), 934–971 (2021)
12. P.F. Antonietti, G. Manzini, S. Scacchi, M. Verani, A review on arbitrarily regular conforming virtual element methods for second- and higher-order elliptic partial differential equations. Math. Models Methods Appl. Sci. **31**(14), 2825–2853 (2021)
13. B. Ayuso de Dios, K. Lipnikov, G. Manzini, The non-conforming virtual element method. ESAIM Math. Model. Numer. **50**(3), 879–904 (2016)
14. J.W. Barrett, S. Langdon, R. Nürnberg, Finite element approximation of a sixth order nonlinear degenerate parabolic equation. Numer. Math. **96**(3), 401–434 (2004)
15. L. Beirão da Veiga, K. Lipnikov, G. Manzini, Arbitrary order nodal mimetic discretizations of elliptic problems on polygonal meshes. SIAM J. Numer. Anal. **49**(5), 1737–1760 (2011)
16. L. Beirão da Veiga, F. Brezzi, A. Cangiani, G. Manzini, L.D. Marini, A. Russo, Basic principles of virtual element methods. Math. Models Methods Appl. Sci. **23**(1), 199–214 (2013)
17. L. Beirão da Veiga, F. Brezzi, L.D. Marini, Virtual elements for linear elasticity problems. SIAM J. Numer. Anal. **51**(2), 794–812 (2013)
18. L. Beirão da Veiga, K. Lipnikov, G. Manzini, in *The Mimetic Finite Difference Method*, ed. MS&A. Modeling, Simulations and Applications, vol. 11, I edn. (Springer, Berlin, 2014)
19. L. Beirão da Veiga, G. Manzini, A virtual element method with arbitrary regularity. IMA J. Numer. Anal. **34**(2), 782–799 (2014).

20. L. Beirão da Veiga, C. Lovadina, D. Mora, A virtual element method for elastic and inelastic problems on polytope meshes. Comput. Methods Appl. Mech. Eng. **295**, 327–346 (2015)
21. L. Beirão da Veiga, G. Manzini, Residual *a posteriori* error estimation for the virtual element method for elliptic problems. ESAIM Math. Model. Numer. Anal. **49**(2), 577–599 (2015)
22. L. Beirão da Veiga, F. Brezzi, L.D. Marini, A. Russo, Mixed virtual element methods for general second order elliptic problems on polygonal meshes. ESAIM. Math. Model. Numer. Anal. **50**(3), 727–747 (2016)
23. L. Beirão da Veiga, F. Brezzi, L.D. Marini, A. Russo, Virtual element methods for general second order elliptic problems on polygonal meshes. Math. Models Methods Appl. Sci. **26**(4), 729–750 (2016)
24. L. Beirão da Veiga, A. Chernov, L. Mascotto, A. Russo, Basic principles of *hp* virtual elements on quasiuniform meshes. Math. Models Methods Appl. Sci. **26**(8), 1567–1598 (2016)
25. L. Beirão da Veiga, A. Chernov, L. Mascotto, A. Russo, Exponential convergence of the *hp* virtual element method in presence of corner singularities. Numer. Math. **138**(3), 581–613 (2018)
26. L. Beirão da Veiga, F. Dassi, A. Russo, A C^1 virtual element method on polyhedral meshes. Comput. Math. Appl. **79**(7), 1936–1955 (2020)
27. L. Beirão da Veiga, F. Dassi, G. Manzini, L. Mascotto, Virtual elements for Maxwell's equations. Comput. Math. Appl. **116**, 82–99 (2022)
28. E. Benvenuti, A. Chiozzi, G. Manzini, N. Sukumar, Extended virtual element method for the Laplace problem with singularities and discontinuities. Comput. Methods Appl. Mech. Eng. **356**, 571–597 (2019)
29. C. Bernardi, M. Dauge, Y. Maday, Polynomials in the Sobolev world. Technical report, HAL (2007). hal-00153795
30. S. Berrone, S. Pieraccini, S. Scialò, F. Vicini, A parallel solver for large scale DFN flow simulations. SIAM J. Sci. Comput. **37**(3), C285–C306 (2015)
31. S. Berrone, A. Borio, Orthogonal polynomials in badly shaped polygonal elements for the virtual element method. Finite Elem. Anal. Des. **129**, 14–31 (2017)
32. S. Berrone, A. Borio, G. Manzini, SUPG stabilization for the nonconforming virtual element method for advection–diffusion–reaction equations. Comput. Methods Appl. Mech. Eng. **340**, 500–529 (2018)
33. M.J. Borden, T.J.R. Hughes, C.M. Landis, C.V. Verhoosel, A higher-order phase-field model for brittle fracture: formulation and analysis within the isogeometric analysis framework. Comput. Methods Appl. Mech. Eng. **273**, 100–118 (2014)
34. J.H. Bramble, R.S. Falk, A mixed-Lagrange multiplier finite element method for the polyharmonic equation. RAIRO Modél. Math. Anal. Numér. **19**(4), 519–557 (1985)
35. S.C. Brenner, R. Scott, *The mathematical theory of finite element methods*, vol. 15 (Springer, Berlin, 2008)
36. F. Brezzi, L.D. Marini, Virtual element methods for plate bending problems. Comput. Methods Appl. Mech. Eng. **253**, 455–462 (2013)
37. F. Brezzi, A. Buffa, K. Lipnikov, Mimetic finite differences for elliptic problems. M2AN Math. Model. Numer. Anal. **43**, 277–295 (2009)
38. F. Brezzi, A. Buffa, G. Manzini, Mimetic scalar products for discrete differential forms. J. Comput. Phys. **257**(Part B), 1228–1259 (2014)
39. F. Brezzi, R.S. Falk, L.D. Marini, Basic principles of mixed virtual element methods. ESAIM Math. Model. Numer. Anal. **48**(4), 1227–1240 (2014)
40. J.W. Cahn, On spinodal decomposition. Acta Metall. **9**, 795–801 (1961)
41. J.W. Cahn, J.E. Hilliard, Free energy of a nonuniform system. I. Interfacial free energy. J. Chem. Phys. **28**, 258–267 (1958)
42. J.W. Cahn, J.E. Hilliard, Free energy of a nonuniform system. III. Nucleation in a two-component incompressible fluid. J. Chem. Phys. **31**, 688–699 (1959)
43. A. Cangiani, G. Manzini, A. Russo, N. Sukumar, Hourglass stabilization of the virtual element method. Internat. J. Numer. Methods Eng. **102**(3–4), 404–436 (2015)

44. A. Cangiani, V. Gyrya, G. Manzini, The non-conforming virtual element method for the Stokes equations. SIAM J. Numer. Anal. **54**(6), 3411–3435 (2016)
45. A. Cangiani, E.H. Georgoulis, T. Pryer, O.J. Sutton, A posteriori error estimates for the virtual element method. Numer. Math. **137**, 857–893 (2017)
46. A. Cangiani, V. Gyya, G. Manzini, O. Sutton, Chapter 14: virtual element methods for elliptic problems on polygonal meshes, in K. Hormann, N. Sukumar, eds. *Generalized Barycentric Coordinates in Computer Graphics and Computational Mechanics* (CRC Press, Taylor & Francis Group, Boca Raton, 2017), pp. 1–20
47. A. Cangiani, G. Manzini, O. Sutton, Conforming and nonconforming virtual element methods for elliptic problems. IMA J. Numer. Anal. **37**, 1317–1354 (2017). (online August 2016)
48. O. Certik, F. Gardini, G. Manzini, G. Vacca, The virtual element method for eigenvalue problems with potential terms on polytopic meshes. Appl. Math. **63**(3), 333–365 (2018)
49. O. Certik, F. Gardini, G. Manzini, L. Mascotto, G. Vacca, The p- and hp-versions of the virtual element method for elliptic eigenvalue problems. Comput. Math. Appl. **79**(7), 2035–2056 (2020)
50. F. Chave, D.A. Di Pietro, F. Marche, F. Pigeonneau, A hybrid high-order method for the Cahn-Hilliard problem in mixed form. SIAM J. Numer. Anal. **54**(3), 1873–1898 (2016)
51. F. Chen, J. Shen, Efficient energy stable schemes with spectral discretization in space for anisotropic Cahn-Hilliard systems. Commun. Comput. Phys. **13**(5), 1189–1208 (2013)
52. L. Chen, X. Huang, Nonconforming virtual element method for $2m$th order partial differential equations in $\mathbb{R}^n$. Math. Comp. **89**(324), 1711–1744 (2020)
53. C. Chinosi, L.D. Marini, Virtual element method for fourth order problems: L^2-estimates. Comput. Math. Appl. **72**(8), 1959–1967 (2016)
54. F. Dassi, L. Mascotto, Exploring high-order three dimensional virtual elements: bases and stabilizations. Comput. Math. Appl. **75**(9), 3379–3401 (2018)
55. D.A. Di Pietro, J. Droniou, G. Manzini, Discontinuous skeletal gradient discretisation methods on polytopal meshes. J. Comput. Phys. **355**, 397–425 (2018)
56. C.M. Elliott, S. Larsson, Error estimates with smooth and nonsmooth data for a finite element method for the Cahn-Hilliard equation. Math. Comp. **58**(198), 603–630, S33–S36 (1992)
57. C.M. Elliott, Z. Songmu, On the Cahn-Hilliard equation. Arch. Rational Mech. Anal. **96**(4), 339–357 (1986)
58. C.M. Elliott, D.A. French, Numerical studies of the Cahn-Hilliard equation for phase separation. IMA J. Appl. Math. **38**(2), 97–128 (1987)
59. C.M. Elliott, D.A. French, A nonconforming finite-element method for the two-dimensional Cahn-Hilliard equation. SIAM J. Numer. Anal. **26**(4), 884–903 (1989)
60. C.M. Elliott, D.A. French, F.A. Milner, A second-order splitting method for the Cahn-Hilliard equation. Numer. Math. **54**(5), 575–590 (1989)
61. E. Faccioli, F. Maggio, A. Quarteroni, A. Taghan, Spectral-domain decomposition methods for the solution of acoustic and elastic wave equations. The Leading Edge **61**, 1160–1174 (1996). Faccioli1996
62. D. Gallistl, Stable splitting of polyharmonic operators by generalized Stokes systems. Math. Comp. **86**(308), 2555–2577 (2017)
63. F. Gardini, G. Manzini, G. Vacca, The nonconforming virtual element method for eigenvalue problems. ESAIM Math. Model. Numer. **53**, 749–774 (2019).
64. F. Gazzola, H.-C. Grunau, G. Sweers, in *Polyharmonic Boundary Value Problems*. Lecture Notes in Mathematics, vol. 1991. (Springer, Berlin, 2010). Positivity preserving and nonlinear higher order elliptic equations in bounded domains.
65. H. Gómez, V.M. Calo, Y. Bazilevs, T.J.R. Hughes, Isogeometric analysis of the Cahn-Hilliard phase-field model. Comput. Methods Appl. Mech. Eng. **197**(49–50), 4333–4352 (2008)
66. P. Grisvard, Elliptic problems in nonsmooth domains, in *Monographs and Studies in Mathematics*, vol. 24. (Pitman (Advanced Publishing Program), Boston, 1985)
67. T. Gudi, M. Neilan, An interior penalty method for a sixth-order elliptic equation. IMA J. Numer. Anal. **31**(4), 1734–1753 (2011)

68. D. Kay, V. Styles, E. Süli, Discontinuous Galerkin finite element approximation of the Cahn-Hilliard equation with convection. SIAM J. Numer. Anal. 47(4), 2660–2685 (2009)
69. D. Komatitsch, J. Tromp, Introduction to the spectral element method for three-dimensional seismic wave propagation. Geophys. J. Int. **139**(3), 806–822 (1999)
70. D.J. Korteweg, Sur la forme que prenent les équations du mouvements des fluides si l'on tient compte des forces capilaires causées par des variations de densité considérables mains continues et sur la théorie de la capillarité dans l'hypothése d'une varation continue de la densité. Arch. Néerl Sci. Exactes Nat. Ser. II (1901)
71. L.D. Landau, On the theory of superconductivity, in D. ter Haar, (ed.) *Collected papers of L. D. Landau*, pp. 546–568 (Pergamon, Oxford, 1965)
72. K. Lipnikov, G. Manzini, A high-order mimetic method for unstructured polyhedral meshes. J. Comput. Phys. **272**, 360–385 (2014)
73. K. Lipnikov, G. Manzini, F. Brezzi, A. Buffa, The mimetic finite difference method for 3D magnetostatics fields problems. J. Comp. Phys. **230**(2), 305–328 (2011)
74. K. Lipnikov, G. Manzini, M. Shashkov, Mimetic finite difference method. J. Comput. Phys. **257**, Part B:1163–1227 (2014)
75. X. Liu, Z. Chen, A virtual element method for the Cahn-Hilliard problem in mixed form. Appl. Math. Lett. **87**, 115–124 (2019)
76. C. Lovadina, D. Mora, I. Velásquez, A virtual element method for the von Kármán equations. Technical report, Preprint CI2MA:2019-36 (2019)
77. G. Manzini, A. Russo, N. Sukumar, New perspectives on polygonal and polyhedral finite element methods. Math. Models Methods Appl. Sci. **24**(8), 1621–1663 (2014)
78. G. Manzini, K. Lipnikov, J.D. Moulton, M. Shashkov, Convergence analysis of the mimetic finite difference method for elliptic problems with staggered discretizations of diffusion coefficients. SIAM J. Numer. Anal. **55**(6), 2956–2981 (2017)
79. L. Mascotto, Ill-conditioning in the virtual element method: stabilizations and bases. Numer. Methods Partial Differential Equations **34**(4), 1258–1281 (2018)
80. D. Mora, I. Velásquez, A virtual element method for the transmission eigenvalue problem. Math. Models Methods Appl. Sci. **28**(14), 2803–2831 (2018)
81. D. Mora, I. Velásquez, Virtual element for the buckling problem of Kirchhoff-Love plates. Comput. Methods Appl. Mech. Eng. **360**, 112687, 22 (2020)
82. D. Mora, G. Rivera, R. Rodríguez, A virtual element method for the Steklov eigenvalue problem. Math. Methods Appl. Sci. **25**(08), 1421–1445 (2015)
83. D. Mora, G. Rivera, I. Velásquez, A virtual element method for the vibration problem of Kirchhoff plates. ESAIM Math. Model. Numer. Anal. **52**(4), 1437–1456 (2018)
84. S. Naranjo-Alvarez, V. Bokil, V. Gyrya, G. Manzini, The virtual element method for resistive magnetohydrodynamics. Comput. Methods Appl. Mech. Eng. **381**, 113815 (2021)
85. K. Park, H. Chi, G.H. Paulino, On nonconvex meshes for elastodynamics using virtual element methods with explicit time integration. Comput. Methods Appl. Mech. Eng. **356**, 669–684 (2019)
86. K. Park, H. Chi, G.H. Paulino, Numerical recipes for elastodynamic virtual element methods with explicit time integration. Internat. J. Numer. Methods Eng. **121**(1), 1–31 (2020)
87. G.H. Paulino, A.L. Gain, Bridging art and engineering using Escher-based virtual elements. Struct. Multidisciplinary Optim. **51**(4), 867–883 (2015)
88. I. Perugia, P. Pietra, A. Russo, A plane wave virtual element method for the Helmholtz problem. ESAIM Math. Model. Num. **50**(3), 783–808 (2016)
89. A. Quarteroni, R. Sacco, F. Saleri, Numerical mathematics, in *Texts in Applied Mathematics*, vol. 37 (Springer, Berlin, 2007)
90. P.-A. Raviart, J.-M. Thomas, *Introduction à l'analyse numérique des équations aux dérivées partielles*. Collection Mathématiques Appliquées pour la Maîtrise. [Collection of Applied Mathematics for the Master's Degree] (Masson, Paris, 1983)
91. B. Rivière, M.F. Wheeler, Discontinuous finite element methods for acoustic and elastic wave problems, in *Current trends in scientific computing (Xi'an, 2002)*. Contemporary Mathematical, vol. 329, pp. 271–282 (American Mathematical Society, Providence, RI, 2003)

92. J.S. Rowlinson, Translation of J. D. van der Waals' "The thermodynamic theory of capillarity under the hypothesis of a continuous variation of density". J. Statist. Phys. **20**(2), 197–244 (1979)
93. M. Schedensack, A new discretization for mth-Laplace equations with arbitrary polynomial degrees. SIAM J. Numer. Anal. **54**(4), 2138–2162 (2016)
94. T. Sorgente, S. Biasotti, G. Manzini, M. Spagnuolo, The role of mesh quality and mesh quality indicators in the virtual element method. Adv. Comput. Math. **48**(3), 1–34 (2022)
95. S. Torabi, J. Lowengrub, A. Voigt, S. Wise, A new phase-field model for strongly anisotropic systems. Proc. R. Soc. Lond. Ser. A Math. Phys. Eng. Sci. **465**(2105), 1337–1359 (2009). With supplementary material available online
96. G. Vacca, Virtual element methods for hyperbolic problems on polygonal meshes. Comput. Math. Appl. **74**(5), 882–898 (2017)
97. M. Wang, J. Xu, Minimal finite element spaces for $2m$-th-order partial differential equations in R^n. Math. Comp. **82**(281), 25–43 (2013)
98. G.N. Wells, E. Kuhl, K. Garikipati, A discontinuous Galerkin method for the Cahn-Hilliard equation. J. Comput. Phys. **218**(2), 860–877 (2006)
99. P. Wriggers, W.T. Rust, B.D. Reddy, A virtual element method for contact. Comput. Mech. **58**(6), 1039–1050 (2016)
100. J. Zhao, S. Chen, B. Zhang, The nonconforming virtual element method for plate bending problems. Math. Models Methods Appl. Sci. **26**(9), 1671–1687 (2016)
101. J. Zhao, B. Zhang, S. Chen, S. Mao, The Morley-type virtual element for plate bending problems. J. Sci. Comput. **76**(1), 610–629 (2018)